Electron transfer through fluctuating bridges: On the validity of the superexchange mechanism and time-dependent tunneling matrix elements

Spiros S. Skourtis,[a] Georgios Archontis,[b] and Qian Xie[c]
Department of Physics, University of Cyprus, P.O. Box 20537, Nicosia 1678, Cyprus

(Received 12 July 2001; accepted 31 August 2001)

The superexchange mechanism of electron-transfer reactions is studied for time-dependent donor–bridge–acceptor systems. It is shown that superexchange may not be a relevant mechanism in a situation where donor and acceptor states are off-resonant to the bridge with an energy gap much greater than K_BT. The competing mechanism in this case involves coherent through-bridge transfer. Methods for estimating its contribution to the electron-transfer probability are presented. It is also shown that the superexchange component of the electron-transfer probability can generally be described by a time-dependent two-state effective Hamiltonian. The off-diagonal element of this Hamiltonian is a generalized superexchange matrix element applicable to time-dependent donor–bridge–acceptor systems. It is nonperturbative and should be used to compute time-dependent superexchange pathways. The derivation of the effective Hamiltonian also applies to time-dependent superexchange systems with multiple donor (acceptor) states. All calculations are carried out on azurin and they involve molecular dynamics simulations coupled to electronic-structure/dynamics calculations using the complete neglect of differential overlap method. © *2001 American Institute of Physics.* [DOI: 10.1063/1.1412874]

I. INTRODUCTION

An important challenge for protein electron-transfer theory is to understand how the dynamics of the protein bridge connecting electron donor to electron acceptor influences the transport of the electron from the donor to acceptor. In the case of nonadiabatic electron transfer mediated by through-bridge tunneling, the electron-transfer rate according to the superexchange model is

$$k_{D\to A}=\frac{2\pi}{\hbar}T_{DA}^2(\mathrm{FC}) \tag{1}$$

(Refs. 1–4). (FC) denotes the nuclear-vibrational Franck–Condon factors between donor and acceptor vibronic manifolds. In the classical limit of nuclear motion (FC) gives rise to a Boltzmann factor for nuclear activation to configurations that cause resonance between donor and acceptor electronic states. T_{DA} is the tunneling-matrix element (superexchange coupling) between the donor and acceptor electronic states at the configuration of resonance. The computation of T_{DA},[5] is the starting point for the calculation of electron-transfer pathways[6] and for any structure-function analysis of the role of the protein bridge in mediating electron transfer.[7] T_{DA} can also be derived from experimental quantities.[8,9]

The dynamics of the protein bridge can lead to exchange of phonons between the tunneling electron and the bridge vibrations and to time-dependent tunneling pathways. Therefore, any structure-function analysis of T_{DA} that is based on a static protein structure may be misleading because it does not provide information about changes in the donor–acceptor coupling that arise from bridge fluctuations. The realization that protein-bridge dynamics may change the nature of tunneling has led to analytical investigations of non-Condon and gating effects on the nonadiabatic rate, and also to calculations that couple the computation of T_{DA} to molecular dynamics simulations of the protein bridge (Refs. 10–19, and see Ref. 20 for a review). Typically, in such calculations a set of static matrix elements is computed from a collection of protein-bridge conformations that are obtained by molecular dynamics simulations. The matrix elements are used either to derive time-dependent tunneling pathways (by doing pathway analysis for each element) or to compute an average donor–acceptor coupling. This approach is very useful for analyzing the robustness of the matrix element (or of a pathway) to changes in the bridge structure. It assumes that the static matrix element description of superexchange electron transfer can be carried over to the time-dependent case by repeating the static analysis at different time instants. As such, it does not incorporate dynamical effects that may arise in a fully time-dependent quantum-mechanical treatment of the electronic problem, where the fluctuations in the nuclear coordinates cause complex time-dependent electronic perturbations of a variety of frequencies and strengths.[21]

Bridge dynamics can also lead to changes in the electron-transfer mechanism from coherent superexchange transport to incoherent thermally activated hopping.[22–24] This transition is relevant to situations where tunneling becomes so slow that thermal activation of the electron from the donor to the bridge and subsequent hopping to the acceptor becomes a competitive mechanism. Long-distance elec-

[a]Author to whom correspondence may be addressed. Electronic mail: skourtis@ucy.ac.cy
[b]Author to whom correspondence may be addressed. Electronic mail: archonti@ucy.ac.cy
[c]Current address: The Concord Consortium, Concord, Massachusetts 01742.

tron transfer systems with small donor(acceptor)–bridge energy gaps are good candidates for observing such a transition. When there is thermally activated transport T_{DA} is irrelevant to the rate and any analysis based on the superexchange coupling (time-dependent or not) is inadequate.

The vast regime between coherent superexchange and incoherent hopping is very rich[24] and largely unexplored. It is relevant to a wide variety of electron-transfer systems (e.g., water, DNA, molecular wires, and molecular scanning tunneling microscopy[25]). Here, theoretical work has focused on cases where an intermediate (bridge) state is transiently resonant to donor and acceptor and the transition from coherent to incoherent transport depends on the relaxation dynamics of the electron in the intermediate state.[26,27] Recent calculations of electronic tunneling through water layers[28] suggest that water structural cavities may support transient resonant states for the electron and thus lead to nonsuperexchange coherent resonant tunneling.

However, not much attention has been paid to nonsuperexchange mechanisms for situations where the bridge states are off-resonant to donor and acceptor at all times, with energy gaps that make incoherent hopping very improbable and coherent resonant tunneling impossible. This regime is the focus of our work, which examines electron transport from a donor to an acceptor state (both of which have fluctuating energies that can cross), through a many-state off-resonant time-dependent bridge. Our goal is to find the most general description of the superexchange mechanism that is valid for time-dependent donor–bridge–acceptor systems and to investigate whether coherent nonsuperexchange mechanisms can contribute significantly to electron transfer prior to the onset of incoherent hopping.

In our calculations the donor–bridge–acceptor system is a segment of the protein azurin[29] (Fig. 1). The nuclear dynamics is classical, obtained from molecular dynamics (MD) simulations on the solvated protein. The time-dependent electronic Hamiltonian of the system is derived from the MD conformations using self-consistent-field (SCF) electronic-structure calculations at the complete neglect of differential overlap (CNDO) level. All computed time-dependent electron-transfer probabilities involve single MD trajectories (there is no ensemble averaging). Any time-averaged quantity is denoted $\langle\ \rangle$. Our results are explained below for a three-state system (prior to the discussion of the many-state case).

A. Description of the main results in terms of a three-state system

First, we reexamine the superexchange model of electron transfer in order to show its limitations and to motivate the analysis that follows. According to this model the effect of the electronic dynamics on the nonadiabatic rate [Eq. (1)] is described by T_{DA}. T_{DA} is computed nonperturbatively by setting it equal to half the minimum energy splitting between two eigenstates of the donor–bridge–acceptor system. These eigenstates are delocalized over donor and acceptor orbitals at the resonance configuration of minimum splitting. Consider a model whereby a donor state (ϕ_D) is weakly coupled to an acceptor state (ϕ_A) via an off-resonant bridge state (ϕ_B). The Hamiltonian is

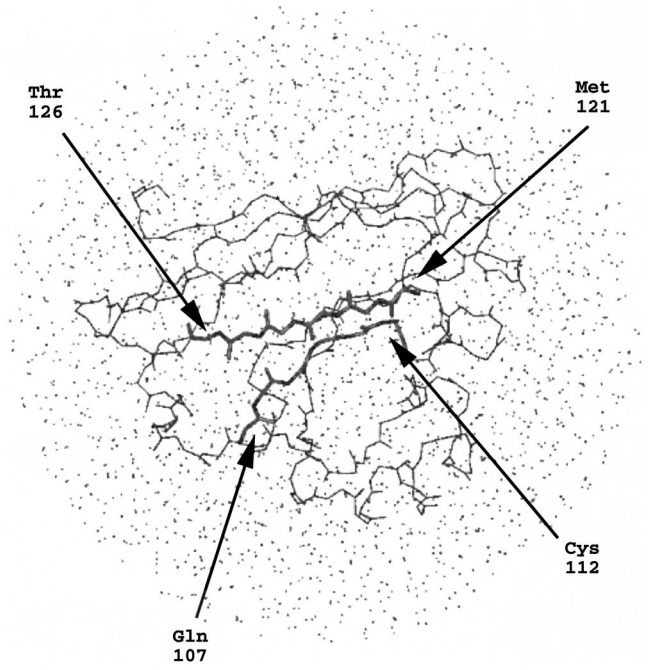

FIG. 1. (a) The protein azurin (Ref. 29) solvated by a layer of water molecules with minimum thickness of 7 Å (only the backbone of the protein is shown). The entire solvated protein is used in the molecular dynamics simulations. The backbone of the β-sheet of azurin consisting of strands 7 and 8 is shown in bold. Molecular dynamics snapshots of the β-sheet at every 1 fs are used for the CNDO-SCF calculations. Tunneling pathway analysis of this β-sheet has been used to analyze electron transfer rates for this protein (Ref. 32).

$$\hat{H}^{3s}(t)=|\phi_D\rangle\epsilon_D\langle\phi_D|+|\phi_A\rangle\epsilon_A\langle\phi_A|+|\phi_B\rangle\epsilon_B\langle\phi_D| +(|\phi_D\rangle v_{DB}\langle\phi_B|+|\phi_A\rangle v_{AB}\langle\phi_B|+\mathrm{h.c.}) \qquad (2)$$

(Fig. 2), where E_i and v_{ij} denote time-dependent state energies and interstate couplings with ϵ_D, $\epsilon_A<\epsilon_B$ and $|v_{AB}/(\epsilon_B-\epsilon_A)|\ll 1$, $|v_{DB}/(\epsilon_B-\epsilon_D)|\ll 1$ (weak coupling to the bridge). The eigenenergies of $\hat{H}^{3s}$ are denoted $E_-<E_+<E_B$ with eigenstates $|\Psi_-\rangle$, $|\Psi_+\rangle$, and $|\Psi_B\rangle$. The eigenstates relevant to the T_{DA} calculation are $|\Psi_-\rangle$ and $|\Psi_+\rangle$. At the resonance configuration ($\epsilon_D\simeq\epsilon_A$) of minimum E_+-E_- their donor and acceptor components are maximized. Namely, in $|\Psi_\pm\rangle=\langle\phi_D|\Psi_\pm\rangle|\phi_D\rangle+\langle\phi_A|\Psi_\pm\rangle|\phi_A\rangle+\langle\phi_B|\Psi_\pm\rangle|\phi_B\rangle$, $|\langle\phi_A|\Psi_\pm\rangle|^2$ and $|\langle\phi_D|\Psi_\pm\rangle|^2\simeq 1/2\gg|\langle\phi_A|\Psi_B\rangle|^2$, $|\langle\phi_D|\Psi_B\rangle|^2$.

Since the superexchange model describes the electronic dynamics in terms of E_+-E_-, it can only describe a mechanism whereby the electron-transfer probability from donor to acceptor is mediated by $|\Psi_-\rangle$ and $|\Psi_+\rangle$. It implicitly assumes that the contribution to the probability of $|\Psi_B\rangle$ is negligible. Suppose that at $t=0$ the initial state of the electron is $|\Psi(0)\rangle=|\phi_D(0)\rangle$. Then, at any time t the exact probability of electron transfer to $|\phi_A(t)\rangle$ is $P_{DA}(t)=|\langle\phi_A(t)|\Psi(t)\rangle|^2$, where $|\Psi(t)\rangle$ (the state of the electron at

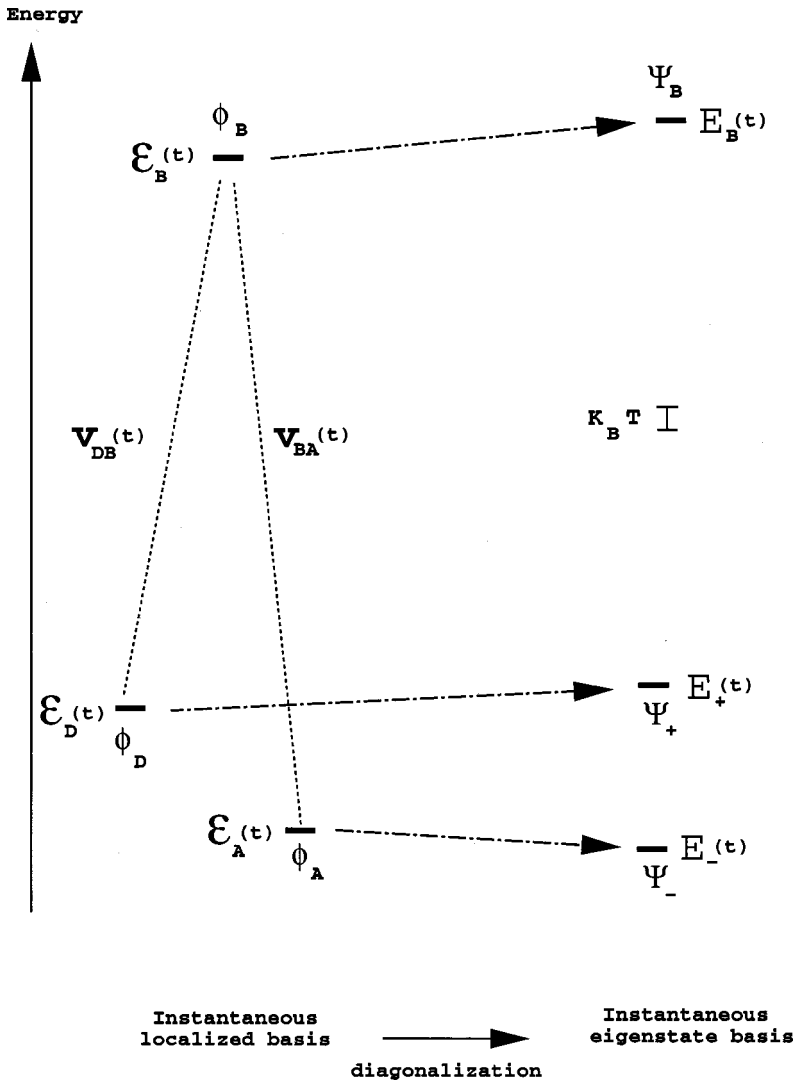

FIG. 2. Left: Diagram showing the site energies $\epsilon_i(t)$ and intersite couplings $v_{ij}(t)$ in $\hat{H}^{3s}(t)$ [Eq. (2)] for the case where the donor state $|\phi_D(t)\rangle$ and the acceptor state $|\phi_A(t)\rangle$ are off-resonant to the bridge state $|\phi_B(t)\rangle$ and $\epsilon_D(t) > \epsilon_A(t)$. Right: Diagram showing the eigenenergies $E_-(t)$, $E_+(t)$, and $E_B(t)$ of $\hat{H}^{3s}(t)$ corresponding to the eigenstates $|\Psi_-(t)\rangle$, $|\Psi_+(t)\rangle$, and $|\Psi_B(t)\rangle$ when there is weak coupling between donor and acceptor with the bridge. The eigenenergies $E_-(t)$ and $E_+(t)$ are separated from $E_B(t)$ and each $E_m(t)$ is slightly shifted from a corresponding $\epsilon_i(t)$ (horizontal arrows). The eigenstates $|\Psi_m(t)\rangle$ are coupled to each other by the matrix elements $K_{mn}^{\mathrm{eig}}(t) = \langle \Psi_n(t)|d_t\Psi_m(t)\rangle = \langle \Psi_n(t)|[d_t\hat{H}^{3s}(t)]|\Psi_m(t)\rangle / (E_m(t) - E_n(t))$ (not shown in the diagram). When $\epsilon_D(t) > \epsilon_A(t)$ and $|\phi_D(t)\rangle$ ($|\phi_A(t)\rangle$) are weakly coupled to $|\phi_B(t)\rangle$, Eq. (39) holds. The eigenstates with the largest and smallest $|\phi_D(t)\rangle$ component are $|\Psi_+(t)\rangle$ and $|\Psi_-(t)\rangle$, respectively, and the eigenstates with the largest and smallest $|\phi_A(t)\rangle$ component are $|\Psi_-(t)\rangle$ and $|\Psi_+(t)\rangle$, respectively. However, when there is resonance between $|\phi_D(t)\rangle$ and $|\phi_A(t)\rangle$ [$\epsilon_D(t) \simeq \epsilon_A(t)$] such that $E_+(t) - E_-(t)$ is minimized, both $|\Psi_-(t)\rangle$ and $|\Psi_+(t)\rangle$ are maximally delocalized among $|\phi_D(t)\rangle$ and $|\phi_A(t)\rangle$ [Eqs. (41) and (42) hold]. In the superexchange model T_{DA} is set equal to $\min(E_+(t) - E_-(t))/2$.

time t) satisfies the time-dependent Schrödinger equation $i\hbar d_t|\Psi(t)\rangle = \hat{H}^{3s}(t)|\Psi(t)\rangle$. Expansion of $|\Psi(t)\rangle$ in terms of $|\Psi_\pm(t)\rangle$ and $|\Psi_B(t)\rangle$ gives

$$P_{DA}(t) = |\langle \phi_A|\Psi_+\rangle\langle\Psi_+|\Psi\rangle + \langle \phi_A|\Psi_-\rangle\langle\Psi_-|\Psi\rangle + \langle \phi_A|\Psi_B\rangle\langle\Psi_B|\Psi\rangle|^2 \quad (3)$$

(where $|\phi_A\rangle$, $|\Psi_m\rangle$ and $|\Psi\rangle$ denote states at time t). The superexchange model is only an approximation to the probability $|\langle \phi_A|\Psi_+\rangle\langle\Psi_+|\Psi\rangle + \langle \phi_A|\Psi_-\rangle\langle\Psi_-|\Psi\rangle|^2$. For example, to arrive at Eq. (1) a Landau–Zener-type approximation can be used. The simplest approximation sets $P_{DA}^{\mathrm{su}}(t) \simeq 1 - \exp[-(2\pi)^2\gamma_{\mathrm{LZ}}(t^*)]$, where $\gamma_{\mathrm{LZ}}(t^*) = T_{DA}(t^*)^2/h|d_t[\epsilon_D(t^*) - \epsilon_A(t^*)]$ is the Landau–Zener parameter and $T_{DA}(t^*)$ is the matrix element obtained from the minimum $E_+ - E_-$ (assumed to occur at $t = t^*$). In the nonadiabatic limit $\gamma_{\mathrm{LZ}} \ll 1$ and $d_t P_{DA}^{\mathrm{su}} \simeq (2\pi)^2\gamma_{\mathrm{LZ}} \propto T_{DA}^2$ [as in Eq. (1)]. Landau–Zener approximations that incorporate multiple t^*[30] have recently been used to compute electron-transfer rates for small bridged molecules, taking into account the full time dependence of the molecule.[31]

The probability $|\langle \phi_A|\Psi_+\rangle\langle\Psi_+|\Psi\rangle + \langle \phi_A|\Psi_-\rangle \times \langle\Psi_-|\Psi\rangle|^2$ is the component of $P_{DA}(t)$ that arises entirely from the eigenstates $|\Psi_\pm(t)\rangle$ and it will be denoted "superexchange" $[P_{DA}^{\mathrm{su}}(t)]$. The exact probability can be written as

$$P_{DA}(t) = P_{DA}^{\mathrm{su}}(t) + \delta P_{DA}(t), \quad (4)$$

where

$$P_{DA}^{\mathrm{su}}(t) = |\langle \phi_A|\Psi_+\rangle\langle\Psi_+|\Psi\rangle + \langle \phi_A|\Psi_-\rangle\langle\Psi_-|\Psi\rangle|^2,$$

and

$$\delta P_{DA}(t) = 2\,\mathrm{Re}\{[\langle \phi_A|\Psi_+\rangle\langle\Psi_+|\Psi\rangle + \langle \phi_A|\Psi_-\rangle \times \langle\Psi_-|\Psi\rangle][\langle \phi_A|\Psi_B\rangle\langle\Psi_B|\Psi\rangle]\} + |\langle \phi_A|\Psi_B\rangle\langle\Psi_B|\Psi\rangle|^2$$

(all states at time t). The implicit assumption behind the superexchange model of electron transfer is that $\delta P_{DA}(t)$ is negligible compared to $P_{DA}^{\mathrm{su}}(t)$. $\delta P_{DA}(t)$ contains the contribution of $|\Psi_B(t)\rangle$.

In this work we will show (for a many-state bridge) that $\delta P_{DA}(t)$ can be larger than $P_{DA}^{\mathrm{su}}(t)$ even in a tunneling regime where ϕ_D and ϕ_A are always off-resonant to the bridge states. For the three-state system the contribution of $\delta P_{DA}(t)$ to the probability is determined by the amplitude

$\langle\phi_A(t)|\Psi_B(t)\rangle\langle\Psi_B(t)|\Psi(t)\rangle$ in Eq. (4) [$\delta P_{DA}(t)$ vanishes if this amplitude vanishes]. We denote $\langle\phi_A(t)|\Psi_B(t)\rangle \times\langle\Psi_B(t)|\Psi(t)\rangle$ the amplitude for "coherent through-bridge transfer." In the eigenstate basis the initial state of the electron is

$$|\Psi(0)\rangle=|\phi_D(0)\rangle=|\Psi_+(0)\rangle\langle\Psi_+(0)|\phi_D(0)\rangle + |\Psi_-(0)\rangle\langle\Psi_-(0)|\phi_D(0)\rangle + |\Psi_B(0)\rangle\langle\Psi_B(0)|\phi_D(0)\rangle. \quad (5)$$

At time t the state has evolved to

$$\begin{aligned}|\Psi(t)\rangle&=\hat{U}(t)|\phi_D(0)\rangle\\ &=\hat{U}(t)|\Psi_+(0)\rangle\langle\Psi_+(0)|\phi_D(0)\rangle\\ &\quad+\hat{U}(t)|\Psi_-(0)\rangle\langle\Psi_-(0)|\phi_D(0)\rangle\\ &\quad+\hat{U}(t)|\Psi_B(0)\rangle\langle\Psi_B(0)|\phi_D(0)\rangle,\end{aligned} \quad (6)$$

where $\hat{U}(t)$ is the time evolution operator for the system [the solution of $i\hbar d_t\hat{U}(t)=\hat{H}^{3s}(t)\hat{U}(t)$]. When $E_B>E_\pm$ at all times and $E_B-E_\pm\gg K_BT$ (Fig. 2), transitions between $|\Psi_B\rangle$ and $|\Psi_\pm\rangle$ are suppressed because the coupling $K^{\rm eig}_{B\pm}(t)=\langle\Psi_B(t)|[d_t\hat{H}^{3s}(t)]|\Psi_\pm(t)\rangle/(E_\pm(t)-E_B(t))$ is negligible. Therefore, in Eq. (6), $\hat{U}(t)|\Psi_B(0)\rangle\simeq$phase$\times|\Psi_B(t)\rangle$ and $\langle\Psi_B(t)|\hat{U}(t)|\Psi_\pm(0)\rangle\simeq 0$, such that

$$\langle\phi_A(t)|\Psi_B(t)\rangle\langle\Psi_B(t)|\Psi(t)\rangle \simeq\text{phase}\times\langle\phi_A(t)|\Psi_B(t)\rangle\langle\Psi_B(0)|\phi_D(0)\rangle. \quad (7)$$

The amplitude for coherent through-bridge transfer is the product of the initial donor component and the final acceptor component of the eigenstate $|\Psi_B\rangle$. It can be computed by solving the time-*independent* Schrödinger equation at the initial and final times.

A lower estimate of the amplitude's magnitude is obtained by calculating the donor and acceptor components of $|\Psi_B\rangle$ in Eq. (7) with first-order perturbation theory. The result is $|\langle\phi_A(t)|\Psi_B(t)\rangle\langle\Psi_B(0)|\phi_D(0)\rangle|\simeq|v_{AB}(t)/(\epsilon_B(t)-\epsilon_A(t))||v_{DB}(0)/(\epsilon_B(0)-\epsilon_D(0))|$. The magnitude is small and we expect $\delta P_{DA}(t)$ to make a significant contribution to $P_{DA}(t)$ only when the superexchange dynamics is very slow such that $P^{\rm su}_{DA}(t)$ is also small. This is possible when there is an activation barrier for the configuration of donor–acceptor resonance and/or $P^{\rm su}_{DA}(t)$ is strongly nonadiabatic. In the latter case all terms in $P_{DA}(t)$ [Eq. (4)] that depend on $|\Psi_\pm\rangle$ are negligible. Therefore, $P_{DA}(t)\simeq|\langle\phi_A(t)|\Psi_B(t)\rangle \times\langle\Psi_B(t)|\Psi(t)\rangle|^2\simeq|\langle\phi_A(t)|\Psi_B(t)\rangle\langle\phi_D(0)|\Psi_B(0)\rangle|^2$ and electron transfer takes place via the coherent through-bridge mechanism.

The perturbative estimate of the coherent through-bridge probability, $|\langle\phi_A(t)|\Psi_B(t)\rangle\langle\Psi_B(t)|\Psi(t)\rangle|^2\simeq|v_{AB}(t)/(\epsilon_B(t)-\epsilon_A(t))|^2|v_{DB}(0)/(\epsilon_B(0)-\epsilon_D(0))|^2$, shows that its magnitude does not depend on $d_t[\epsilon_D-\epsilon_A]$. Rather, it is determined by the average energetics of the system because the fluctuations in ϵ_i and v_{ij} are small compared to the average energy gap between ϵ_B and $\epsilon_{D(A)}$ in the regime considered here. Although the magnitude is small, it is greater than the probability of thermal hopping from ϕ_D to the bridge. The simulations described in the following sections show that $|\langle\phi_A|\Psi_B\rangle\langle\Psi_B|\Psi\rangle|^2\sim10^{-5}$–$10^{-4}$ for an energy gap of ~1–2 eV, whereas the probability of thermal hopping would be $\exp(-\beta[1\,\text{eV}])\sim10^{-18}$. Therefore, if the electron-transfer reaction becomes strongly nonadiabatic, as in the case of large donor–acceptor distances, this coherent mechanism of transfer will take over from the coherent superexchange mechanism prior to the onset of incoherent through-bridge hopping. Coherent through-bridge transfer is enhanced if the donor(acceptor)–bridge energy gap is reduced because there is greater delocalization of the donor and acceptor states into the bridge [larger $\langle\phi_A|\Psi_B\rangle$ and $\langle\phi_D|\Psi_B\rangle$ in Eq. (7)]. It is an independent mechanism from superexchange as long as the donor and acceptor energies lie in the bridge HOMO–LUMO gap such that transitions between $|\Psi_\pm\rangle$ and $|\Psi_B\rangle$ are suppressed. It is also an independent mechanism from through-bridge hopping as long as $E_B(t)-E_\pm(t)>K_BT$ (Fig. 2).

The definition of the superexchange mechanism, $P^{\rm su}_{DA}(t)$ in Eq. (4), is very general because $|\Psi_\pm(t)\rangle$ are eigenstates of the entire donor–bridge–acceptor system. However, the form of $P^{\rm su}_{DA}(t)$ given in Eq. (4) is difficult to compute because it requires propagating $|\Psi_\pm(t)\rangle$ with the time-dependent Schrödinger equation in the eigenstate basis. The difficulty arises from the large size of a typical electron-transfer calculation and from the behavior of the coupling between $|\Psi_+\rangle$ and $|\Psi_-\rangle$ at the resonance configurations where E_+-E_- is minimized. The coupling $K^{\rm eig}_{+-}(t)\propto(E_+(t)-E_-(t))^{-1}$ behaves as a delta function at these configurations for long-distance electron transfer (where $E_+-E_-\to0$). In addition to these computational problems there is also a question of interpretation. The form of $P^{\rm su}_{DA}(t)$ in Eq. (4) cannot be readily associated with a two-state system consisting of a donor state that is coupled to an acceptor state by some bridge-mediated matrix element. We will show that an effective localized two-state description of $P^{\rm su}_{DA}(t)$ is possible. The effective two-state system is comprised of time-dependent "renormalized" donor and acceptor states that are coupled by a time-dependent matrix element. This two-state description provides a method for computing $P^{\rm su}_{DA}(t)$ by solving a reduced (2×2) time-dependent Schrödinger equation. Therefore, it avoids the problem of size and, due to the use of a localized basis, the problem of delta-function behavior. It generalizes the concept of superexchange matrix element (and pathways) to systems of arbitrary time dependence without making Landau–Zener-type approximations that may not be justifiable for time-dependent bridges (Sec. V).

B. The many-state case

In the calculations that follow we investigate electron transfer through a fluctuating donor–protein bridge–acceptor system without *a priori* assumptions about the validity of the superexchange mechanism and of the effective tunneling matrix element description of electron transfer. The exact electron-transfer probability between donor and acceptor states is computed as a function of time using the time-

dependent Hamiltonian of the entire donor–bridge–acceptor system. The type of Hamiltonian considered is of the general form

$$\hat{H}(t)=\hat{H}_{DA}(t)+\hat{H}_{\mathrm{br}}(t)+\hat{H}_{DA-\mathrm{br}}(t), \tag{8}$$

where

$$\begin{aligned}\hat{H}_{DA}(t)&=|\phi_D\rangle\epsilon_D\langle\phi_D|+|\phi_A\rangle\epsilon_A\langle\phi_A|\\&\quad+(|\phi_D\rangle v_{DA}\langle\phi_A|+\mathrm{h.c.}),\\ \hat{H}_{\mathrm{br}}(t)&=\sum_i\ |\phi_i^{\mathrm{br}}\rangle\epsilon_i^{\mathrm{br}}\langle\phi_i^{\mathrm{br}}|+\sum_{i>j}\ (|\phi_i^{\mathrm{br}}\rangle v_{ij}^{\mathrm{br}}\langle\phi_j^{\mathrm{br}}|+\mathrm{h.c.}),\\ \hat{H}_{DA-\mathrm{br}}(t)&=\sum_i\ (|\phi_D\rangle v_{Di}\langle\phi_i^{\mathrm{br}}|+\mathrm{h.c.})\\&\quad+\sum_j\ (|\phi_A\rangle v_{Aj}\langle\phi_i^{\mathrm{br}}|+\mathrm{h.c.}),\end{aligned} \tag{9}$$

and ϕ_D, ϕ_A, and $\{\phi_i^{\mathrm{br}}\}$ denote D, A, and $N-2$ bridge localized orbitals (to be described later) with orbital site energies ϵ_i and interorbital couplings v_{ij} (all time dependent). The electron transfer probability between $\phi_D(t)$ and $\phi_A(t)$ is given by

$$P_{DA}(t)=|\langle\phi_A(t)|\Psi(t)\rangle|^2. \tag{10}$$

$|\Psi(t)\rangle$ is the state of the donor–bridge–acceptor system, satisfying the time-dependent Schrödinger equation (TDSE)

$$i\hbar\frac{d}{dt}|\Psi(t)\rangle=\hat{H}(t)|\Psi(t)\rangle,\qquad \text{where}\ \ |\Psi(0)\rangle=|\phi_D(0)\rangle. \tag{11}$$

The exact probability $P_{DA}(t)$ is studied as a function of donor–acceptor distance and donor/acceptor energy in order to address the following question: under what circumstances is it possible to approximate $P_{DA}(t)$ by use of an effective two-state Hamiltonian that is the time-dependent generalization of the static superexchange model? To this end we seek an effective two-state (donor–acceptor) Hamiltonian $\hat{H}^{2s}(t)$ that can be computed at each instant from two of the instantaneous eigenstates/eigenenergies of the system, i.e., eigenstates satisfying the time-independent Schrödinger equation (TISE)

$$\hat{H}(t)|\Psi_m(t)\rangle=E_m(t)|\Psi_m(t)\rangle. \tag{12}$$

Further, we require that propagation with a two-state TDSE using $\hat{H}^{2s}(t)$, i.e., with

$$i\hbar\frac{d}{dt}|\Psi^{2s}(t)\rangle=\hat{H}^{2s}(t)|\Psi^{2s}(t)\rangle,\qquad \text{where}\ \ |\Psi^{2s}(0)\rangle=|\phi_D(0)\rangle, \tag{13}$$

produces a probability

$$P_{DA}^{2s}(t)=|\langle\phi_A(t)|\Psi^{2s}(t)\rangle|^2, \tag{14}$$

that approximates the exact $P_{DA}(t)$ for a given time interval.

It is shown that in tunneling situations an effective Hamiltonian

$$\begin{aligned}\hat{H}^{2s}(t)&=|\phi_D(t)\rangle H_{DD}^{2s}(t)\langle\phi_D(t)|+|\phi_A(t)\rangle H_{AA}^{2s}(t)\\&\quad\times\langle\phi_A(t)|+(|\phi_D(t)\rangle H_{DA}^{2s}(t)\langle\phi_A(t)|+\mathrm{h.c.}),\end{aligned} \tag{15}$$

can be found for a wide range of parameters. However, as the donor–acceptor separation is increased at constant average donor and acceptor energies, $P_{DA}^{2s}(t)$ computed from $\hat{H}^{2s}(t)$ becomes a progressively worse approximation to $P_{DA}(t)$ within a fixed time window. This is explained by showing that $P_{DA}^{2s}(t)$ only describes the superexchange component $P_{DA}^{\mathrm{su}}(t)$ of $P_{DA}(t)$ and that at large donor–acceptor separations $P_{DA}^{\mathrm{su}}(t)$ becomes very small (due to the strong nonadiabaticity of the reaction). At large separations the exact probability is determined by a competing nonsuperexchange component that involves eigenstates of the system with bridge (rather than donor–acceptor) character. This component is the generalization (to many states) of the mechanism of coherent through-bridge transfer discussed in the previous section. Since $\hat{H}^{2s}(t)$ describes $P_{DA}^{\mathrm{su}}(t)$, its off-diagonal element should be interpreted as a generalized superexchange matrix element $[T_{DA}(t)\equiv H_{DA}^{2s}(t)]$. Its diagonal elements are renormalized time-dependent donor and acceptor energies (e.g., $H_{DD}^{2s}(t)=\epsilon_D(t)+\delta\epsilon_D^{\mathrm{re}}(t)$).

In Sec. II we describe how the two-state effective Hamiltonian is constructed and how the two-state and exact electron-transfer probabilities are computed [Eqs. (10) and (14)]. Details of the calculations on the protein azurin are given. Section III is a study of the two-state and exact probabilities (within a ps time window) as a function of donor–acceptor separation at fixed average donor and acceptor energies. The failure of the two-state probability at large separations is explained by demonstrating the slowing down of the superexchange component of the probability. In Sec. IV the two-state time-dependent Schrödinger equation [Eq. (13)] is derived from the exact (N-state) Schrödinger equation [Eq. (11)] in order to obtain the necessary conditions for the validity of the effective-Hamiltonian approximation. All assumptions made in the derivation are tested numerically as a function of average donor and acceptor energies and donor–acceptor separation. Generalized notation is used in the derivation to show that all arguments can be generalized to tunneling situations with more than two donor(acceptor) states. In the final section we discuss ways of estimating the relative contributions to the electron-transfer probability of the coherent through-bridge and superexchange channels without having to compute the exact probability (an impossible task for a large system). This is important because, in a situation where the coherent through-bridge channel dominates the electron-transfer dynamics, time-dependent superexchange pathways are irrelevant. We also discuss the implications of the existence of this channel for the behavior of electron transfer as a function of distance and temperature. Finally, for cases where the superexchange channel is dominant, we show how to derive time-dependent pathways from the effective two-state Hamiltonian and discuss how their analysis and interpretation depends on the crossing dynamics of the effective donor and acceptor states.

II. SIMULATION OF THE EXACT AND THE TWO-STATE PROBABILITIES

To describe the calculations of the exact and two-state probability for the fluctuating protein system, we switch to matrix notation and assume that the basis of localized orbitals $\{\phi_i(t)\}$ is orthonormal. The matrix form of the N-state TDSE [Eq. (11)] in the localized basis $\{\phi_i(t)\}$ is

$$i\hbar \frac{d}{dt}\mathbf{C}^{\mathrm{loc}}(t)=[\mathbf{H}^{\mathrm{loc}}(t)-i\hbar\mathbf{K}^{\mathrm{loc}}(t)]\mathbf{C}^{\mathrm{loc}}(t), \tag{16}$$

where

$$\begin{aligned} H_{ij}^{\mathrm{loc}}(t)&=\langle\phi_i(t)|\hat{H}(t)|\phi_j(t)\rangle,\\ K_{ij}^{\mathrm{loc}}(t)&=\langle\phi_i(t)|d_t\phi_j(t)\rangle \end{aligned} \tag{17}$$

[$\hat{H}$ given in Eq. (9)], and

$$\mathbf{C}^{\mathrm{loc}}(t)=\begin{pmatrix} C_D^{\mathrm{loc}}(t)\\ C_A^{\mathrm{loc}}(t)\\ \cdot\\ C_{\mathrm{br}_i}^{\mathrm{loc}}(t)\\ \cdot \end{pmatrix}, \tag{18}$$

with $C_i^{\mathrm{loc}}(t)=\langle\phi_i(t)|\Psi(t)\rangle$.

In terms of the state vector $\mathbf{C}^{\mathrm{loc}}(t)$, the transition probability from donor to acceptor [Eq. (10)] is

$$P_{DA}(t)=|C_A^{\mathrm{loc}}(t)|^2 \quad \text{given} \quad C_i^{\mathrm{loc}}(0)=\delta_{iD}. \tag{19}$$

The matrix form of the TISE [Eq. (12)] in the localized basis is

$$\mathbf{H}^{\mathrm{loc}}(t)\boldsymbol{\Psi}_m(t)=E_m(t)\boldsymbol{\Psi}_m(t), \tag{20}$$

where $\boldsymbol{\Psi}_m(t)$ denotes the mth instantaneous eigenvector of the system, i.e.,

$$\boldsymbol{\Psi}_m(t)=\begin{pmatrix} \Psi_{Dm}(t)\\ \Psi_{Am}(t)\\ \cdot\\ \Psi_{im}(t)\\ \cdot \end{pmatrix}, \tag{21}$$

with $\Psi_{im}(t)=\langle\phi_i(t)|\Psi_m(t)\rangle$.

The computation of $P_{DA}(t)$ [Eq. (19)] is carried out by coupled molecular dynamics (MD) and electronic-structure/dynamics calculations on the protein azurin.[29]

A. Molecular dynamics

The system employed in the molecular dynamics simulations consists of an entire azurin molecule[29] with its native copper ion, and several thousand explicit water molecules. To account for the effect of solvent on the protein dynamics, the crystallographic water molecules are retained. Additional water molecules are included to produce a hydration layer with minimum thickness of 7 Å. To create this layer, a pre-equilibrated 28 Å water sphere is overlayed on the azurin monomer and the water that overlaps with protein-heavy atoms or crystallographic water oxygen atoms is deleted. This overlaying procedure is repeated two more times during the course of molecular dynamics equilibration, giving a total of 2448 water molecules. Atomic charges, van der Waals- and force-field parameters for the protein were taken from the CHARMM22 all-atom force field.[33] The water is reproduced by a modified TIP3P water model.[34]

The copper ion forming the native metal center of azurin is interacting strongly with residues His-46(N), His-117(N), and Cys-112(S), and has weaker interactions with residues Met-121(S) and Gly-45(O). The geometry of the complex can be described as distorted bipyramidal, with the first three liganded donor atoms in the equatorial plane and the last two in axial positions. Following earlier work on the blue copper protein plastocyanin,[35] the copper atom is modeled to be bound to the first three residues; the interactions with the last two residues are reproduced by nonbonded energy terms. The force field for the copper complex is similar to the one employed in Ref. 35. Electrostatic interactions are calculated by use of a multipole approximation for groups more than 13 Å apart;[36] van der Waals interactions are switched to zero at distances larger than 12 Å. Water molecules are restrained to a spherical region of 28 Å radius by the stochastic boundary method.[37] Heavy atoms outside a sphere of 24 Å are subjected to random and frictional forces mimicking a thermal bath at 293 K.[38] Bond lengths with hydrogen atoms, and the geometry of water molecules are constrained by the SHAKE algorithm.[39] The classical equations of motion are integrated by a Verlet algorithm modified for Langevin dynamics, using a time step of 1 fs.

After an initial equilibration for 300 ps, a large number of 1-ps dynamics segments are chosen from a production trajectory with duration of several hundred ps. Atomic coordinates of the β-sheet segment (strands 7 and 8, Fig. 1) are extracted from the simulation trajectories. The ruptured peptide groups at the two backbone ends of the isolated segment are completed with standard blocking methyl groups, taken from the CHARMM topology file.

B. Electronic dynamics

The atomic coordinates of the β sheet are stored at every 1 fs and used to compute the converged CNDO-SCF[40] density and Fock matrices of the β sheet at each fs, as in Ref. 21. The Fock matrix $\mathbf{F}(t)$ is expressed in the basis set $\{\phi_i(t)\}$ of all natural lone-pair and two-center bonding and antibonding orbitals of the β sheet. These are derived by one-center and two-center block diagonalization of the density matrix[41] using a modified version[21] of the original BONDO procedure.[42] To compute the exact probability for a given MD segment for a wide range of donor–acceptor separations and energies, a pair of C_α–H natural bonds of the β sheet is chosen as the $\phi_D(t)$ and $\phi_A(t)$ orbitals. At each fs the site energies $\mathbf{F}_{DD}(t)$ and $\mathbf{F}_{AA}(t)$ are shifted by the same constant energy ϵ inside the bridge HOMO–LUMO gap. The shift creates site energies $\epsilon_D(t)=\mathbf{F}_{DD}(t)+\epsilon$ and $\epsilon_A(t)=\mathbf{F}_{AA}(t)+\epsilon$ that ensure tunneling transport between $\phi_D(t)$ and $\phi_A(t)$ (rather than hopping transport). The resulting Fock matrix for the particular MD segment is the donor–bridge–acceptor Hamiltonian $\mathbf{H}^{\mathrm{loc}}(t)$ [Eq. (17) and Fig. 3(a)] that is utilized for the computation of $P_{DA}(t)$ [Eq. (19)]. This computation is carried out by propagating the N-state TDSE [Eq. (16)] with a predictor–corrector procedure. A time step of $\sim 10^{-3}$ fs must be used in order to obtain stable solutions. For time instants

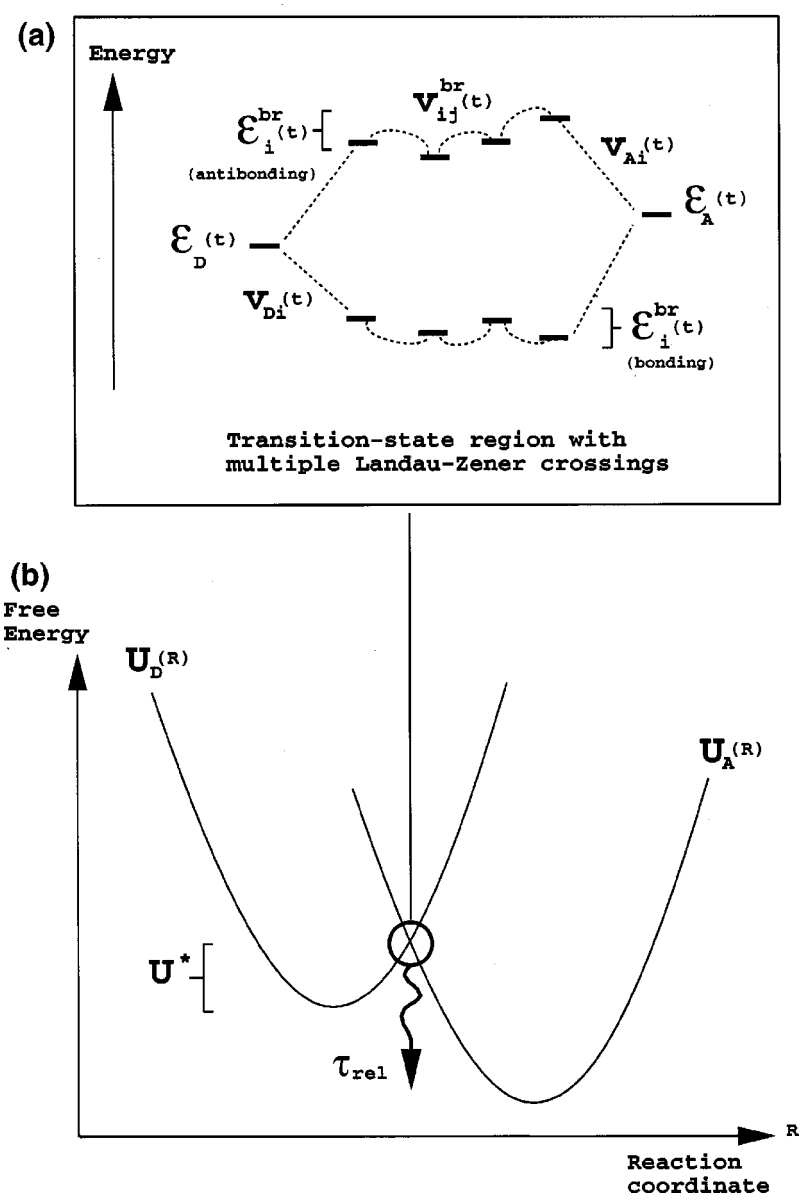

FIG. 3. (a) Schematic diagram showing the fluctuating site energies (bold lines) and intersite couplings (dotted lines) for the localized orbitals ϕ_i, as described by the Hamiltonian $\mathbf{H}^{\mathrm{loc}}(t)$ [Eqs. (17) and (8), (9)]. The time dependence of all Hamiltonian matrix elements is computed from coupled MD/CNDO-SCF simulations on the β-sheet of azurin (Fig. 1). The localized orbitals are natural bonding and antibonding orbitals. The energies of ϕ_D and ϕ_A are shown inside the bridge HOMO–LUMO gap. They undergo multiple Landau–Zener crossings and in all simulations $\epsilon_D=\epsilon_A$ at $t=0$. (b) The simulations [energy level diagram of (a)] is interpreted as a model for electron transfer with multiple Landau–Zener crossings between donor and acceptor at the crossing region of the donor and acceptor free-energy surfaces. Therefore, the maximum time scale of observation of the $P_{DA}(t)$ is determined by the average time scale of relaxation out of the crossing region. Relaxation out of the crossing region and reactivation are not modeled by our simulations.

between successive fs (MD) snapshots, all $H_{ij}^{\mathrm{loc}}(t)$ matrix elements are computed by cubic spline interpolation. In the CNDO implementation of Eq. (16), the terms $K_{ij}(t)=\langle\phi_i(t)|d_t\phi_j(t)\rangle$ are ignored since the CNDO approximation itself ignores the overlap matrix $S_{ij}(t)=\langle\phi_i(t)|\phi_j(t)\rangle$ in the diagonalization of the secular equation. The effect of the $\mathbf{K}^{\mathrm{loc}}(t)$ matrix on propagating the N-state TDSE was tested using an extended Huckel[43] procedure and it was found to be negligible.[21]

Given the N-state Hamiltonian $\mathbf{H}^{\mathrm{loc}}(t)$ and probability $P_{DA}(t)$ for a particular MD segment, we compute the two-state probability $P_{DA}^{2s}(t)$ [to be compared with $P_{DA}(t)$] by use of a time-dependent two-state Hamiltonian matrix $\mathbf{H}^{2s}(t)$. At each time t we search for two eigenstates of $\mathbf{H}^{\mathrm{loc}}(t)$ that have the largest ϕ_D and ϕ_A components, i.e., for each of these two eigenstates $|\Psi_{Dm}(t)|^2$ and/or $|\Psi_{Am}(t)|^2$ must be maximized [Eq. (21)]. The existence of two such eigenstates in the gap of the system's eigenspectrum is guaranteed if $\phi_D(t)$ and $\phi_A(t)$ lie in the bridge HOMO–LUMO gap and are sufficiently weakly coupled to the bridge.[44–46] Denoting these eigenstates $\mathbf{\Psi}_+(t)$ and $\mathbf{\Psi}_-(t)$ and their ϕ_D/ϕ_A components $\Psi_{A\pm}(t)\,\Psi_{D\pm}(t)$ [Eqs. (20), (21)], we define $\mathbf{H}^{2s}(t)$ as

$$\mathbf{H}^{2s}(t)=\begin{pmatrix} H_{DD}^{2s}(t) & H_{DA}^{2s}(t) \\ H_{AD}^{2s}(t) & H_{AA}^{2s}(t) \end{pmatrix} \equiv \begin{pmatrix} A(t) & B(t) \\ B(t) & -A(t) \end{pmatrix} \begin{pmatrix} E_+(t) & 0 \\ 0 & E_-(t) \end{pmatrix} \times \begin{pmatrix} A(t) & B(t) \\ B(t) & -A(t) \end{pmatrix}^{-1}, \tag{22}$$

where $E_+(t)$ and $E_-(t)$ are the eigenenergies of $\mathbf{\Psi}_+(t)$ and $\mathbf{\Psi}_-(t)$, and

$$A(t)=\frac{\Psi_{D+}(t)}{\sqrt{|\Psi_{D+}(t)|^2+|\Psi_{A+}(t)|^2}},$$
$$B(t)=\frac{\Psi_{A+}(t)}{\sqrt{|\Psi_{D+}(t)|^2+|\Psi_{A+}(t)|^2}} \tag{23}$$

(Ref. 47). Then, to obtain $P_{DA}^{2s}(t)$ for the MD segment, we propagate the two-state TDSE

$$i\hbar\frac{d}{dt}\underbrace{\begin{pmatrix}C_D^{2s}(t)\\C_A^{2s}(t)\end{pmatrix}}_{\mathbf{C}^{2s}(t)}=\underbrace{\begin{pmatrix}H_{DD}^{2s}(t) & H_{DA}^{2s}(t)\\H_{AD}^{2s}(t) & H_{AA}^{2s}(t)\end{pmatrix}}_{\mathbf{H}^{2s}(t)}\underbrace{\begin{pmatrix}C_D^{2s}(t)\\C_A^{2s}(t)\end{pmatrix}}_{\mathbf{C}^{2s}(t)}$$
$$\text{where } C_i^{2s}(0)=\delta_{iD}, \tag{24}$$

and set

$$P_{DA}^{2s}(t)=|C_D^{2s}(t)|^2 \tag{25}$$

(details of the derivation of the approximation are given in Sec. IV). As with Eq. (16), the TDSE in Eq. (24) is solved using the predictor–corrector method with a time step of 10^{-3} fs. In terms of $|\Psi^{2s}(t)\rangle$ and $\hat{H}^{2s}(t)$ in Eqs. (14) and (13), $C_D^{2s}(t)=\langle\phi_D(t)|\Psi^{2s}(t)\rangle$, $C_A^{2s}(t)=\langle\phi_A(t)|\Psi^{2s}(t)\rangle$, and $H_{ij}^{2s}(t)=\langle\phi_i(t)|\hat{H}^{2s}(t)|\phi_j(t)\rangle$, $(i(j)=D,A)$. $\mathbf{H}^{2s}(t)$ is chosen such that, at any time of resonance between the donor and acceptor states ($t=t^*$), the energy splitting between the instantaneous eigenstates of $\mathbf{H}^{2s}(t^*)$ is equal to twice the tunneling matrix element that would be computed in a nonperturbative static calculation (where the system is frozen at its t^* conformation).

III. THE BEHAVIOR OF THE EXACT AND TWO-STATE PROBABILITIES AS A FUNCTION OF $\phi_D-\phi_A$ DISTANCE AND NONADIABATICITY

A large number of simulations of $P_{DA}(t)$ and $P_{DA}^{2s}(t)$ have been performed as a function of $\phi_D-\phi_A$ separation and using different MD segments. The locations of the ϕ_D and ϕ_A bond orbitals chosen for these simulations are both within a single β-sheet strand (to probe covalent-bond pathways) and in different strands (to probe hydrogen-bond pathways). All probabilities shown in the figures are obtained from single MD segments and are neither time-nor ensemble averaged.

Figure 4 summarizes a representative set of simulations of $P_{DA}(t)$ (light line) and $P_{DA}^{2s}(t)$ (bold line) for a given MD segment and as a function of $\phi_D-\phi_A$ separation. Each horizontal pair of plots shows the initial 200 fs and 1 ps dynamics of $P_{DA}(t)$ and $P_{DA}^{2s}(t)$ corresponding to a specific $\phi_D-\phi_A$ pair along a single strand of the β sheet (shown on the right). All simulations (a)–(e) share a common ϕ_D orbital (ϕ_D is the C_α–H bond of Met-121) and have identical initial ϕ_D and ϕ_A energies (-10 eV) and equal average ϕ_D and ϕ_A site energies ($\langle\epsilon_D\rangle\simeq\langle\epsilon_A\rangle\simeq-10$ eV[48]). The only difference between the successive pairs of plots (a)–(e) is the ϕ_A orbital. ϕ_A is the C_α–H bond of the following residues: (a) Lys-122; (b) Gly-123; (c) Thr-124; (d) Leu-125; (e) Thr-126, chosen progressively further away from Met-121. The rightmost side of the figure shows the rms averages of the tunneling matrix element $H_{DA}^{2s(\mathrm{rms})}$ and Landau–Zener parameter $\gamma_{\mathrm{LZ}}^{(\mathrm{rms})}$ for each simulation (a)–(e). Both quantities are defined using the effective two-state approximation. For the tunneling matrix element

$$H_{DA}^{2s(\mathrm{rms})}=\sqrt{\frac{1}{N_c}\sum_{i=1}^{N_c}[H_{DA}^{2s}(t_i^*)]^2}, \tag{26}$$

where H_{DA}^{2s} is the off-diagonal element of the effective Hamiltonian obtained from $\mathbf{H}^{\mathrm{loc}}(t)$ using Eqs. (22) and (23). H_{DA}^{2s} is evaluated at the N_c crossing times of the diagonal elements of the effective Hamiltonian [i.e., at all $\{t_i^*\}$ within 1 ps with $H_{DD}^{2s}(t_i^*)=H_{AA}^{2s}(t_i^*)$]. Similarly, for the Landau–Zener parameter

$$\gamma_{\mathrm{LZ}}^{(\mathrm{rms})}=\sqrt{\frac{1}{N_c}\sum_{i=1}^{N_c}[\tau_{\mathrm{LZ}}(t_i^*)/\tau_{\mathrm{Rabi}}(t_i^*)]^2}, \tag{27}$$

where

$$\begin{aligned}\tau_{\mathrm{LZ}}(t_i^*)/\tau_{\mathrm{Rabi}}(t_i^*)&=[H_{DA}^{2s}(t_i^*)]^2/\hbar\left|d_t[H_{DD}^{2s}(t_i^*)-H_{AA}^{2s}(t_i^*)]\right|\\ \tau_{\mathrm{LZ}}(t_i^*)&\equiv|H_{DA}^{2s}(t_i^*)|/|d_t[H_{DD}^{2s}(t_i^*)-H_{AA}^{2s}(t_i^*)]|,\\ \tau_{\mathrm{Rabi}}(t_i^*)&\equiv\hbar/|H_{DA}^{2s}(t_i^*)|.\end{aligned} \tag{28}$$

The plots in Fig. 4 show that within 1 ps the electron-transfer probability decreases with increasing $\phi_D-\phi_A$ separation [from $\langle P_{DA}(t)\rangle_{1\mathrm{ps}}\simeq0.5$ in Fig. 4(a) to $\langle P_{DA}(t)\rangle_{1\mathrm{ps}}\simeq10^{-5}$ in Fig. 4(e)]. This is expected since the average energies of ϕ_D and ϕ_A are kept constant inside the bridge HOMO–LUMO gap. A more important observation is that $\langle P_{DA}(t)\rangle_{1\mathrm{ps}}$ drops to its lowest magnitude ($\simeq10^{-5}$) for the intermediate $\phi_D-\phi_A$ separation [Fig. 4(c)], and it is insensitive to a further increase in the separation [Figs. 4(d) and 4(e)]. The second observation relates to the approximate $P_{DA}^{2s}(t)$ compared to the exact $P_{DA}(t)$. $P_{DA}^{2s}(t)$ becomes more nonadiabatic with increasing $\phi_D-\phi_A$ separation [$\gamma_{\mathrm{LZ}}^{(\mathrm{rms})}$ ranges from 6.9×10^{-2} in Fig. 4(a) to 2.2×10^{-11} in Fig. 4(e)], and simultaneously it becomes a worse approximation to $P_{DA}(t)$. For $\gamma_{\mathrm{LZ}}^{(\mathrm{rms})}<10^{-8}$, $P_{DA}^{2s}(t)\ll P_{DA}(t)$ within 1 ps. For example, in Fig. 4(e) $\max\{P_{DA}^{2s}(t)\}_{1\mathrm{ps}}\simeq10^{-8}$ and $\langle P_{DA}(t)\rangle_{1\mathrm{ps}}\simeq10^{-5}$. Since the MD trajectory and the initial conditions in Figs. 4(a)–4(e) are identical, the large discrepancy between $P_{DA}^{2s}(t)$ and $P_{DA}(t)$ for $\gamma_{\mathrm{LZ}}^{(\mathrm{rms})}<10^{-8}$ arises from a slowing down of $P_{DA}^{2s}(t)$ with increasing nonadiabaticity. The slowing down of $P_{DA}^{2s}(t)$ is confirmed by use of the formula

$$\max\{P_{DA}^{2s}(t)\}\simeq N_c(2\pi)^2\gamma_{\mathrm{LZ}}^{(\mathrm{rms})}. \tag{29}$$

The right-hand side of Eq. (29) is an approximation to the total Landau–Zener probability for the case of multiple incoherent Landau–Zener crossings, each of $\gamma_{\mathrm{LZ}}\ll1$.[30] Equation (29) predicts the value of $\max\{P_{DA}^{2s}(t)\}$ when the average Landau–Zener parameter is much less than unity [e.g., in Fig. 4 it predicts the observed $\max\{P_{DA}^{2s}(t)\}$ for all cases (b)–(e)]. The validity of Eq. (29) indicates that $P_{DA}^{2s}(t)$ in Figs. 4(b)–4(e) describes electron transfer that takes place in incoherent steps at the donor–acceptor crossing times $\{t_i^*\}$ of the effective two-state system. The probability of electron

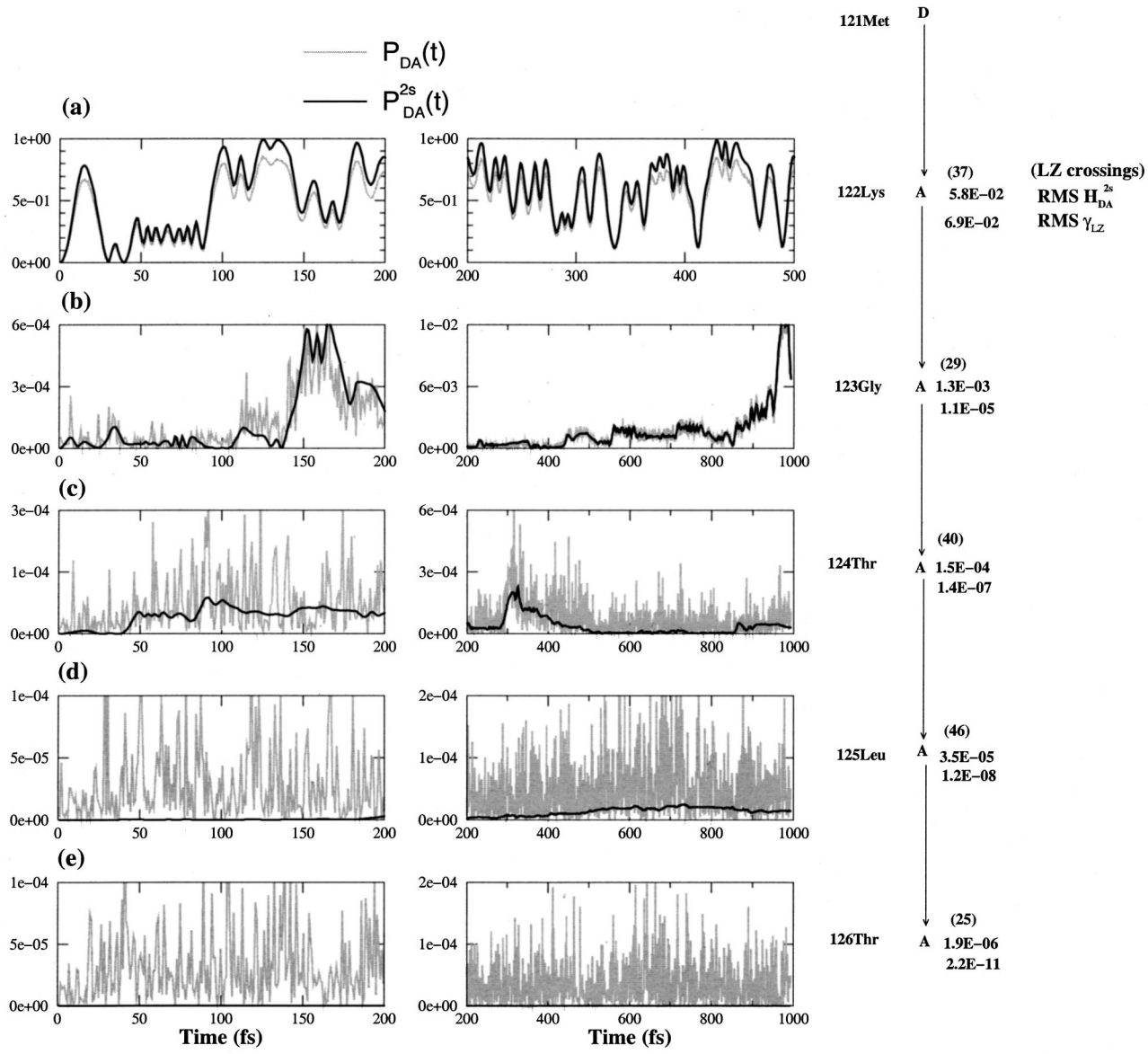

FIG. 4. $P_{DA}(t)$ in Eq. (19) and $P^{2s}_{DA}(t)$ in Eq. (25) as a function of $\phi_D-\phi_A$ separation and at constant average ϵ_D and ϵ_A energies. The ϕ_D orbital chosen for each simulation (a)–(e) is the C_α–H natural bond of Met-121, and the ϕ_A orbital is the C_α–H natural bond of: (a) Lys-122; (b) Gly-123; (c) Thr-124; (d) Leu-125; (e) Thr-126. The left half of the figure shows horizontally for each ϕ_D/ϕ_A pair the short (200 fs) and longer time (200 fs–1 ps) dynamics of $P_{DA}(t)$ (dotted line) and $P^{2s}_{DA}(t)$ (bold line). For (a) only the dynamics up to 500 fs is shown because it does not change at later times. Next to these plots is a schematic diagram of the relevant β-sheet strand, indicating the amino acid location of each ϕ_A orbital with respect to Met-121 (where ϕ_D is located). The rightmost side of the figure shows, for each simulation (a)–(e), the rms value of the superexchange matrix element [Eq. (26)] and of the Landau–Zener parameter [Eq. (27)]. The latter is obtained from the time-dependent two-state Hamiltonian that gives rise to $P^{2s}_{DA}(t)$ [Eqs. (22) and (23)]. Also shown in parentheses is the total number of crossing times t_i^* between the effective donor and acceptor energies (the diagonal elements of the two-state Hamiltonian). All simulations (a)–(e) are carried out using the same MD trajectory for the β-sheet, identical initial condition [$\epsilon_D(0)=\epsilon_A(0)=-10$ eV], and similar average energetics ($\langle E^{\rm bri}_{\rm homo}\rangle \simeq -12$ eV, $\langle E^{\rm bri}_{\rm lumo}\rangle \simeq 2$ eV, and $\langle\epsilon_D\rangle\simeq\langle\epsilon_A\rangle\simeq-10$ eV). In (e) $P^{2s}_{DA}(t)$ is not visible because it is much smaller than $P_{DA}(t)$. In (b)–(e) the maximum value of $P^{2s}_{DA}(t)$ within 1 ps [$\max\{P^{2s}_{DA}(t)\}$] is given by the rms value of the Landau–Zener parameter through Eq. (29).

transfer at each t_i^* is proportional to $\gamma_{\rm LZ}(t_i^*)$, i.e., to the ratio of the Landau–Zener time to the Rabi time at t_i^*. As this ratio decreases, $P^{2s}_{DA}(t)$ slows down.

In summary, when the dynamics of $P_{DA}(t)$ is observed within a finite time interval, it may not be determined by the two-state $P^{2s}_{DA}(t)$, even though $\epsilon_D(t)$ and $\epsilon_A(t)$ lie in the HOMO–LUMO gap of the system. This happens when $P^{2s}_{DA}(t)$ increases very slowly due to strong nonadiabaticity of the electron-transfer reaction. In such a case $P_{DA}(t)$ is determined by a mechanism that makes it robust to changes in the $\phi_D-\phi_A$ separation (at constant $\langle\epsilon_D\rangle$ and $\langle\epsilon_A\rangle$). The nature of this mechanism is explained below.

A. Competition between gap-eigenstate (superexchange) and bridge-eigenstate transfer

We analyze the exact donor amplitude $C^{\rm loc}_A(t)=\langle\phi_A(t)|\Psi(t)\rangle$ [used to compute $P_{DA}(t)=|C^{\rm loc}_A(t)|^2$] in terms of the exact gap-eigenstate amplitudes $\langle\Psi_+(t)|\Psi(t)\rangle$ and $\langle\Psi_-(t)|\Psi(t)\rangle$ of the N-state system. The exact gap eigenstates and eigenenergies are used to construct the effec-

tive two-state Hamiltonian $\mathbf{H}^{2s}(t)$ that give rise to $P_{DA}^{2s}(t)$. Therefore, the discrepancy between $P_{DA}^{2s}(t)$ and $P_{DA}(t)$ for the larger $\phi_D-\phi_A$ separations should be understood using this analysis.

In general, the state vector of the system in the localized-orbital basis [$\mathbf{C}^{\mathrm{loc}}(t)$ in Eq. (18)], can be written as

$$\mathbf{C}^{\mathrm{loc}}(t)=\mathbf{\Psi}(t)\mathbf{C}^{\mathrm{eig}}(t). \tag{30}$$

In Eq. (30) $\mathbf{\Psi}(t)=(\mathbf{\Psi}_{m_1}(t),\ldots,\mathbf{\Psi}_{m_N}(t))$ is the matrix of all instantaneous eigenvectors [Eq. (21)] and $\mathbf{C}^{\mathrm{eig}}(t)$ is the state vector of the system in the instantaneous-eigenstate basis, i.e.,

$$\mathbf{C}^{\mathrm{eig}}(t)=\begin{pmatrix}\cdot\\ C_m^{\mathrm{eig}}(t)\\ \cdot\end{pmatrix}, \quad \text{where } C_m^{\mathrm{eig}}(t)=\langle\Psi_m(t)|\Psi(t)\rangle. \tag{31}$$

The dynamics of $\mathbf{C}^{\mathrm{eig}}(t)$ is determined by the TDSE

$$i\hbar\frac{d}{dt}\mathbf{C}^{\mathrm{eig}}(t)=[\mathbf{H}^{\mathrm{eig}}(t)-i\hbar\mathbf{K}^{\mathrm{eig}}(t)]\mathbf{C}^{\mathrm{eig}}(t), \tag{32}$$

where

$$H_{nm}^{\mathrm{eig}}(t)=\delta_{nm}E_m(t) \quad \text{and} \quad K_{nm}^{\mathrm{eig}}(t)=\langle\Psi_n(t)|d_t\Psi_m(t)\rangle. \tag{33}$$

Using Eq. (30), $C_A^{\mathrm{loc}}(t)$ can be separated into $\mathbf{\Psi}_{\pm}(t)$ and $\mathbf{\Psi}_{m\neq\pm}$ contributions, i.e.,

$$C_A^{\mathrm{loc}}(t)=\overbrace{\Psi_{A+}(t)C_+^{\mathrm{eig}}(t)+\Psi_{A-}(t)C_-^{\mathrm{eig}}(t)}^{C_A^{\mathrm{su}}(t)} + \overbrace{\sum_{m\neq\pm}\Psi_{Am}(t)C_m^{\mathrm{eig}}(t)}^{C_A^{\mathrm{bri}}(t)}. \tag{34}$$

The gap-eigenstate contribution to $C_A^{\mathrm{loc}}(t)$ is denoted "superexchange" [$C_A^{\mathrm{su}}(t)$]. The contribution of the remaining eigenstates [$C_A^{\mathrm{bri}}(t)$] is denoted "bridge" because, for each system eigenstate $\mathbf{\Psi}_{m\neq\pm}$, the $\{\phi_i^{\mathrm{br}}\}$ component of $\mathbf{\Psi}_m$ is much greater than the ϕ_D/ϕ_A component (i.e., $\Sigma_{i\neq D,A}|\Psi_{im}|^2\gg|\Psi_{Dm}|^2+|\Psi_{Am}|^2$). Using Eq. (34), the exact probability is written as

$$P_{DA}(t)=P_{DA}^{\mathrm{su}}(t)+\delta P_{DA}(t), \tag{35}$$

where

$$P_{DA}^{\mathrm{su}}(t)=|C_A^{\mathrm{su}}(t)|^2,$$

and

$$\delta P_{DA}(t)=2\,\mathrm{Re}[C_A^{\mathrm{su}}(t)^*C_A^{\mathrm{bri}}(t)]+|C_A^{\mathrm{bri}}(t)|^2 \tag{36}$$

[generalization of Eq. (4)]. It should be emphasized that $C_A^{\mathrm{su}}(t)$ [$P_{DA}^{\mathrm{su}}(t)$] described above is not exactly the same quantity as $C_A^{2s}(t)$ [$P_{DA}^{2s}(t)$] in Eqs. (24) and (25). $C_A^{\mathrm{su}}(t)$ is defined in terms of the exact gap-eigenstate amplitudes $C_+^{\mathrm{eig}}(t)$ and $C_-^{\mathrm{eig}}(t)$, derived by propagating the N-state TDSE [Eq. (32)]. $C_+^{\mathrm{eig}}(t)$ and $C_-^{\mathrm{eig}}(t)$ therefore take into account transitions between $\mathbf{\Psi}_{\pm}(t)$ and $\mathbf{\Psi}_{m\neq\pm}(t)$. Such transitions are not incorporated in $C_A^{2s}(t)$, which is computed (starting at $t=0$) by a two-state TDSE [Eq. (24)]. This is further explained in Sec. IV.

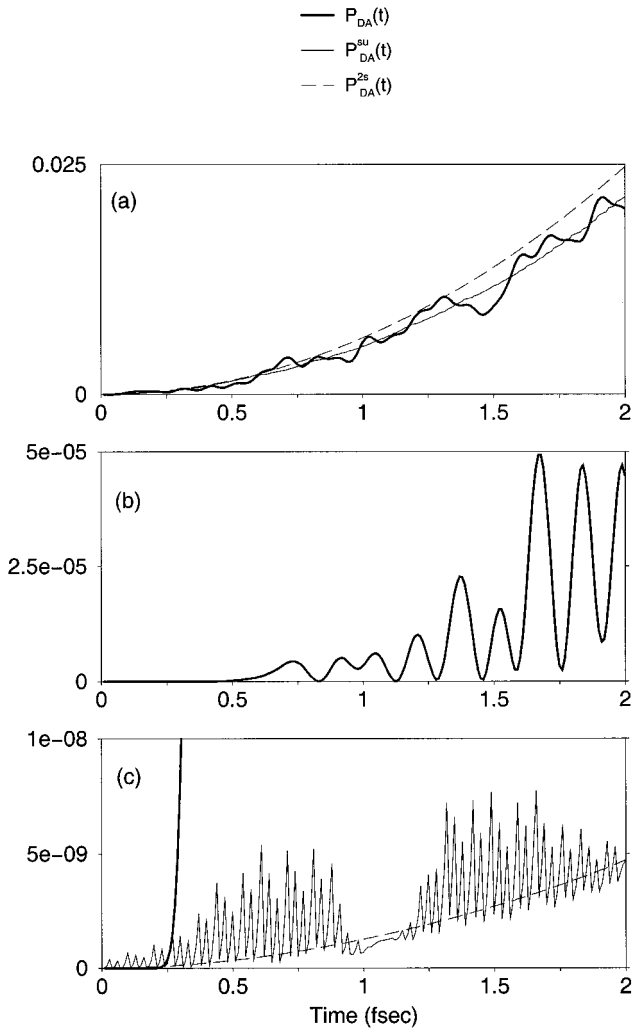

FIG. 5. (a) The exact $P_{DA}(t)$ [Eq. (19)] vs $P_{DA}^{\mathrm{su}}(t)$ [Eqs. (34)–(36)] and $P_{DA}^{2s}(t)$ [Eq. (25)], for the initial 2 fs of the system in Fig. 4(a) ($\phi_D-\phi_A$ pair: Met-121–Lys-122). (b) The exact $P_{DA}(t)$ for the initial 2 fs of the system in Fig. 4(d) ($\phi_D-\phi_A$ pair: Met-121–Leu-125). (c) The exact $P_{DA}(t)$ vs $P_{DA}^{\mathrm{su}}(t)$ and $P_{DA}^{2s}(t)$ for the same system as in (b).

Figure 5(a) shows the initial dynamics of $P_{DA}(t)$, $P_{DA}^{\mathrm{su}}(t)$, and $P_{DA}^{2s}(t)$ for the $\phi_D-\phi_A$ pair of Fig. 4(a) (Met-121–Lys-122). For this $\phi_D-\phi_A$ separation $P_{DA}^{\mathrm{su}}(t)$ is a very good approximation to $P_{DA}(t)$, indicating that superexchange transport as defined in Eqs. (34)–(36) dominates the electron-transfer probability. $P_{DA}^{2s}(t)$ is a good approximate description of $P_{DA}^{\mathrm{su}}(t)$ and, therefore, it also approximates $P_{DA}(t)$ [as seen in Fig. 4(a)]. Figure 5(b) shows the initial dynamics for the system in Fig. 4(d) (Met-121–Leu-125). Although the $\phi_D-\phi_A$ separation is much larger than in the previous example, the MD trajectory, $\phi_D(t)$, $\epsilon_D(t)$, $\epsilon_A(0)$, and $\langle\epsilon_D\rangle$ and $\langle\epsilon_A\rangle$ are the same. In this case $P_{DA}(t)$ rises very fast to its average magnitude of $\langle P_{DA}(t)\rangle_{1\mathrm{ps}}\simeq 10^{-5}$ [see Fig. 4(d)], whereas the superexchange component $P_{DA}^{\mathrm{su}}(t)$ is negligible. $P_{DA}^{2s}(t)$ still approximates $P_{DA}^{\mathrm{su}}(t)$ but now it cannot describe $P_{DA}(t)$.

In conclusion, for the longer $\phi_D-\phi_A$ separations in Fig.

TABLE I. Partitioning in localized basis.

State vector	Subvector	Elements
$\mathbf{C}^{\mathrm{loc}}$	$\mathbf{C}_p^{\mathrm{loc}}$	C_D^{loc}, C_A^{loc}
	$\mathbf{C}_q^{\mathrm{loc}}$	$\{C_i^{\mathrm{loc}}\}$, $i=\phi_i^{\mathrm{br}}$
Matrix $\mathbf{M}$	Submatrix	Elements M_{ij}
$\mathbf{H}^{\mathrm{loc}}$ or $\mathbf{K}^{\mathrm{loc}}$	$\mathbf{M}_{pp}$	$i=\phi_D,\phi_A$ $j=\phi_D,\phi_A$
	$\mathbf{M}_{pq}$	$i=\phi_D,\phi_A$ $j=\phi_j^{\mathrm{br}}$
	$\mathbf{M}_{qq}$	$i=\phi_i^{\mathrm{br}}$ $j=\phi_j^{\mathrm{br}}$

TABLE III. Partitioning in mixed localized-eigenstate basis.

mth eigenstate vector	Subvector	Elements
$\mathbf{\Psi}_m$	$\mathbf{\Psi}_{pm}$	Ψ_{Dm}, Ψ_{Am}
	$\mathbf{\Psi}_{qm}$	$\{\Psi_{im}\}$, $i=\phi_i^{\mathrm{br}}$
Eigenstate matrix	Submatrices ($m=\pm$)	Submatrices ($m\neq\pm$)
$\mathbf{\Psi}=(\mathbf{\Psi}_{m_1},\ldots\mathbf{\Psi}_{m_N})$	$\mathbf{\Psi}_{pr}=(\mathbf{\Psi}_{p+},\mathbf{\Psi}_{p-})$	$\mathbf{\Psi}_{ps}=(\mathbf{\Psi}_{pm_1},\ldots\mathbf{\Psi}_{pm_{N-2}})$
	$\mathbf{\Psi}_{qr}=(\mathbf{\Psi}_{q+},\mathbf{\Psi}_{q-})$	$\mathbf{\Psi}_{qs}=(\mathbf{\Psi}_{qm_1},\ldots\mathbf{\Psi}_{qm_{N-2}})$

4 where $P_{DA}(t)\gg P_{DA}^{\mathrm{su}}(t)$, the dynamics of $P_{DA}(t)$ is not determined by the gap eigenstates of the system but rather by the remaining eigenstates $\mathbf{\Psi}_{m\neq\pm}(t)$ that have bridge character. The time-dependent two-state approximation, a description of the gap-eigenstate contribution to $P_{DA}(t)$, fails when this contribution becomes negligible. In the following sections it is shown that the fast rise of $P_{DA}(t)$ for the longer $\phi_D-\phi_A$ separations arises from the nonzero electron amplitude in the eigenstates $\mathbf{\Psi}_{m\neq\pm}$ at $t=0$ [$\Sigma_{m\neq\pm}\langle\phi_D(0)|\Psi_{m\neq\pm}(0)\rangle>0$]. This amplitude propagates along the bridge to ϕ_A in a manner similar to resonant transport so that it does not decay fast with increasing $\phi_D-\phi_A$ separation.

IV. DERIVATION OF THE TWO-STATE TDSE

The two-state TDSE [Eq. (24)] is derived using generalized notation in order to demonstrate that the derivation applies for effective time-dependent Hamiltonians of dimension higher than two. The basis set of localized orbitals $\{\phi_i\}$ is partitioned into the relevant subspace of the ϕ_D and ϕ_A orbitals (denoted p), and the subspace of bridge ϕ_i^{br} orbitals (denoted q) (Table I and the Appendix). The basis set of instantaneous eigenstates $|\Psi_m\rangle$ is partitioned into the relevant subspace (r) of the gap eigenstates $|\Psi_+\rangle$ and $|\Psi_-\rangle$ that are used in the two-state approximation, and the subspace (s) of all remaining eigenstates (Table II and the Appendix).

The starting point for the derivation of the two-state TDSE is an N-state TDSE

$$i\hbar\frac{d}{dt}\mathbf{C}^{\mathrm{loc}}(t)=[\mathbf{\Psi}(t)\mathbf{H}^{\mathrm{eig}}(t)-i\hbar\mathbf{K}^{\mathrm{loc}}(t)\mathbf{\Psi}(t)]\mathbf{C}^{\mathrm{eig}}(t), \tag{37}$$

which relates the dynamics of the state vector in the basis of localized states to the dynamics of the state vector in the instantaneous-eigenstate basis [derived by differentiating Eq. (30)]. The relevant component of $d_t\mathbf{C}^{\mathrm{loc}}(t)$ in Eq. (37) is $d_t\mathbf{C}_p^{\mathrm{loc}}(t)$, which contains the elements $d_tC_D^{\mathrm{loc}}(t)=d_t\langle\phi_D(t)|\Psi(t)\rangle$ and $d_tC_A^{\mathrm{loc}}(t)=d_t\langle\phi_A(t)|\Psi(t)\rangle$. Separating the gap-eigenstate contribution to $d_t\mathbf{C}_p^{\mathrm{loc}}(t)$ from the contribution of the remaining eigenstates gives

$$i\hbar\frac{d}{dt}\mathbf{C}_p^{\mathrm{loc}}(t)=[\mathbf{\Psi}_{pr}\mathbf{H}_{rr}^{\mathrm{eig}}-i\hbar(\mathbf{K}^{\mathrm{loc}}\mathbf{\Psi})_{pr}]\mathbf{C}_r^{\mathrm{eig}}+[\mathbf{\Psi}_{ps}\mathbf{H}_{ss}^{\mathrm{eig}}-i\hbar(\mathbf{K}^{\mathrm{loc}}\mathbf{\Psi})_{ps}]\mathbf{C}_s^{\mathrm{eig}} \tag{38}$$

[for the explanation of the notation in Eq. (38) see Tables I–III and the Appendix]. In the right-hand side of Eq. (38), the first part describes the dynamics of the donor and acceptor amplitudes that arises from the gap eigenstates $|\Psi_+\rangle$ and $|\Psi_-\rangle$. The second part describes the dynamics that arises from the remaining eigenstates. The two-state TDSE is derived below from Eq. (38). The validity of all assumptions made in the derivation is tested numerically at the end of this section.

For all $\phi_D-\phi_A$ pairs considered in Fig. 4 there are only two eigenstates [$\mathbf{\Psi}_+(t)$ and $\mathbf{\Psi}_-(t)$] and two localized states [$\phi_D(t)$ and $\phi_A(t)$] with energies in the gap region of the system's eigenspectrum. In this situation time-independent perturbation theory guarantees that, for each gap eigenstate $\mathbf{\Psi}_\pm$, either the ϕ_D component or the ϕ_A component is large or, alternatively, both of these components are large. In the first case [relevant when $\phi_D(t)$ and $\phi_A(t)$ are off-resonant and weakly coupled]

$$|\Psi_{D+}(t)|^2\gg\sum_{m\neq\pm}|\Psi_{Dm}(t)|^2\gg|\Psi_{D-}(t)|^2 \tag{39}$$

and

$$|\Psi_{A-}(t)|^2\gg\sum_{m\neq\pm}|\Psi_{Am}(t)|^2\gg|\Psi_{A+}(t)|^2$$

[if $\epsilon_D(t)>\epsilon_A(t)$ as in Fig. 2], or

$$|\Psi_{D-}(t)|^2\gg\sum_{m\neq\pm}|\Psi_{Dm}(t)|^2\gg|\Psi_{D+}(t)|^2 \tag{40}$$

and

$$|\Psi_{A+}(t)|^2\gg\sum_{m\neq\pm}|\Psi_{Am}(t)|^2\gg|\Psi_{A-}(t)|^2$$

[if $\epsilon_D(t)<\epsilon_A(t)$]. In the second case [relevant when $\phi_D(t)$ and $\phi_A(t)$ are quasiresonant/strongly coupled]

TABLE II. Partitioning in eigenstate basis.

State vector	Subvector	Elements
$\mathbf{C}^{\mathrm{eig}}$	$\mathbf{C}_r^{\mathrm{eig}}$	C_+^{eig}, C_-^{eig}
	$\mathbf{C}_s^{\mathrm{eig}}$	$\{C_m^{\mathrm{eig}}\}$, $m\neq+,-$
Matrix $\mathbf{M}$	Submatrix	Elements M_{mn}
$\mathbf{H}^{\mathrm{eig}}$ or $\mathbf{K}^{\mathrm{eig}}$	$\mathbf{M}_{rr}$	$m=+,-$ $n=+,-$
	$\mathbf{M}_{rs}$	$m=+,-$ $n\neq+,-$
	$\mathbf{M}_{ss}$	$m\neq+,-$ $n\neq+,-$

$$|\Psi_{D+}(t)|^2 \quad \text{and} \quad |\Psi_{D-}(t)|^2 \gg \sum_{m\neq\pm} |\Psi_{Dm}(t)|^2, \tag{41}$$

and *simultaneously*

$$|\Psi_{A+}(t)|^2 \quad \text{and} \quad |\Psi_{A-}(t)|^2 \gg \sum_{m\neq\pm} |\Psi_{Am}(t)|^2 \tag{42}$$

(see Fig. 2 for an explanation in terms of a three-state system). In Eqs. (39)–(42), the magnitude of the ϕ_D (ϕ_A) component for each gap eigenstate is measured with respect to the total magnitude of the component for all other (nongap) eigenstates.

To derive the two-state TDSE, it is first assumed that Eqs. (41) and (42) are satisfied for the time interval of interest (that includes $t=0$). Then, since $|\Psi(0)\rangle = |\phi_D(0)\rangle$

$$|C_+^{\rm eig}(0)|^2 \quad \text{and} \quad |C_-^{\rm eig}(0)|^2 \gg \sum_{m\neq\pm} |C_m^{\rm eig}(0)|^2 > 0, \tag{43}$$

i.e., the initial population of $\mathbf{\Psi}_+$ and $\mathbf{\Psi}_-$ is much larger than the initial total population of all $\mathbf{\Psi}_{m\neq\pm}$ (the latter being nonzero because the system is not in an eigenstate at $t=0$).

The initial eigenstate populations evolve with time according to Eq. (32) (the TDSE in the eigenstate basis), which is written as

$$i\hbar \frac{d}{dt}\mathbf{C}_r^{\rm eig}(t) = [\mathbf{H}_{rr}^{\rm eig} - i\hbar \mathbf{K}_{rr}^{\rm eig}]\mathbf{C}_r^{\rm eig} - i\hbar \mathbf{K}_{rs}^{\rm eig}\mathbf{C}_s^{\rm eig}$$

and

$$i\hbar \frac{d}{dt}\mathbf{C}_s^{\rm eig}(t) = [\mathbf{H}_{ss}^{\rm eig} - i\hbar \mathbf{K}_{ss}^{\rm eig}]\mathbf{C}_s^{\rm eig} - i\hbar \mathbf{K}_{sr}^{\rm eig}\mathbf{C}_r^{\rm eig}. \tag{44}$$

Equation (44) describes two coupled channels involving the gap-eigenstate amplitudes and the amplitudes of all remaining eigenstates. The matrix elements of $\mathbf{K}_{rs}^{\rm eig}$ and $\mathbf{K}_{sr}^{\rm eig}$ in Eq. (44), $K_{m\pm}^{\rm eig}(t) = \langle \Psi_{m\neq\pm}(t)|d_t\Psi_\pm(t)\rangle$, couple $\mathbf{\Psi}_\pm$ to the remaining $\mathbf{\Psi}_m$. The second assumption in the derivation of the two-state TDSE is that these matrix elements are small, i.e.,

$$\rho_{m\pm}(t) \equiv \left|\frac{\hbar K_{m\pm}^{\rm eig}(t)}{E_m(t)-E_\pm(t)}\right| = \left|\frac{\hbar\langle \Psi_m(t)|[d_t\hat{H}(t)]|\Psi_\pm(t)\rangle}{(E_m(t)-E_\pm(t))^2}\right| \ll 1. \tag{45}$$

This assumption is valid if the energy difference between $\mathbf{\Psi}_\pm$ and any $\mathbf{\Psi}_{m\neq\pm}$ remains large as a function of time. If Eq. (45) is satisfied, $\mathbf{K}_{rs}^{\rm eig}$ and $\mathbf{K}_{sr}^{\rm eig}$ in Eq. (44) can be ignored, leading to two uncoupled channels

$$i\hbar \frac{d}{dt}\mathbf{C}_r^{\rm eig}(t) \simeq [\mathbf{H}_{rr}^{\rm eig} - i\hbar \mathbf{K}_{rr}^{\rm eig}]\mathbf{C}_r^{\rm eig}$$

and (46)

$$i\hbar \frac{d}{dt}\mathbf{C}_s^{\rm eig}(t) \simeq [\mathbf{H}_{ss}^{\rm eig} - i\hbar \mathbf{K}_{ss}^{\rm eig}]\mathbf{C}_s^{\rm eig}.$$

Equation (46) implies that the total gap-eigenstate population $|\mathbf{C}_r^{\rm eig}(t)|^2 = |C_+^{\rm eig}(t)|^2 + |C_m^{\rm eig}(t)|^2$ evolves independently from the total population of the remaining eigenstates $|\mathbf{C}_s^{\rm eig}(t)|^2 = \Sigma_{m\neq\pm}|C_m^{\rm eig}(t)|^2$. Therefore, if $|\mathbf{C}_r^{\rm eig}(0)|^2 \gg |\mathbf{C}_s^{\rm eig}(0)|^2$ [as follows from Eq. (43)], then

$$|\mathbf{C}_r^{\rm eig}(t)|^2 \gg |\mathbf{C}_s^{\rm eig}(t)|^2, \tag{47}$$

for $t>0$ as long as $\rho_{m\pm} \ll 1$ [Eq. (45)].

To relate the eigenstate dynamics to the ϕ_D and ϕ_A dynamics, we consider the TDSE in Eq. (38). The implication of Eqs. (41) and (42) for this TDSE is that the matrix elements of $\mathbf{\Psi}_{pr}(t)$ ($\Psi_{D\pm}, \Psi_{A\pm}$) in Eq. (38) are much larger than the matrix elements of $\mathbf{\Psi}_{ps}(t)$ ($\{\Psi_{Dm}, \Psi_{Am}\}$). If in addition Eq. (45) is satisfied [leading to Eq. (47)], the elements of $\mathbf{C}_r^{\rm eig}(t)$ in Eq. (38) are much larger than the elements of $\mathbf{C}_s^{\rm eig}(t)$. Therefore, the second term in Eq. (38) is negligible with respect to the first term and it can be ignored.[49] The final result is

$$\underbrace{i\hbar \frac{d}{dt}\begin{pmatrix} C_D^{\rm loc}(t) \\ C_A^{\rm loc}(t)\end{pmatrix}}_{i\hbar d_t \mathbf{C}_p^{\rm loc}} \simeq \underbrace{\begin{pmatrix} \Psi_{D+}(t) & \Psi_{D-}(t) \\ \Psi_{A+}(t) & \Psi_{A-}(t)\end{pmatrix}}_{\mathbf{\Psi}_{pr}} \times \underbrace{\begin{pmatrix} E_+(t) & 0 \\ 0 & E_-(t)\end{pmatrix}}_{\mathbf{H}_{rr}^{\rm eig}} \underbrace{\begin{pmatrix} C_+^{\rm eig}(t) \\ C_-^{\rm eig}(t)\end{pmatrix}}_{\mathbf{C}_r^{\rm eig}}. \tag{48}$$

Equation (48) becomes the two-state TDSE [Eq. (24)] if $\mathbf{\Psi}_{pr}(t)$ is replaced by a unitary $\mathbf{\Psi}_{pr}^{\rm un}(t) \simeq \mathbf{\Psi}_{pr}(t)$. This substitution is valid when Eqs. (41) and (42) are satisfied.[50] One such unitary matrix is

$$\mathbf{\Psi}_{pr}^{\rm un}(t) = \begin{pmatrix} A(t) & B(t) \\ B(t) & -A(t)\end{pmatrix}, \tag{49}$$

where $A(t)$ and $B(t)$ are given in Eq. (23). Replacing $\mathbf{\Psi}_{pr}(t)$ with $\mathbf{\Psi}_{pr}^{\rm un}(t)$ in Eq. (48) gives

$$i\hbar d_t \mathbf{C}_p^{\rm loc}(t) \simeq \mathbf{\Psi}_{pr}^{\rm un}\mathbf{H}_{rr}^{\rm eig}[\mathbf{\Psi}_{pr}^{\rm un}]^{-1}\mathbf{\Psi}_{pr}^{\rm un}\mathbf{C}_r^{\rm eig}. \tag{50}$$

This is the two-state TDSE [Eq. (24)] where

$$\mathbf{\Psi}_{pr}^{\rm un}(t)\mathbf{H}_{rr}^{\rm eig}(t)[\mathbf{\Psi}_{pr}^{\rm un}(t)]^{-1} = \mathbf{H}^{2s}(t), \tag{51}$$

and $\mathbf{C}^{2s}(t) = \mathbf{\Psi}_{pr}^{\rm un}(t)\mathbf{C}_r^{\rm eig}(t)$ is the state vector in the ϕ_D/ϕ_A basis, renormalized such that there is no leakage to the bridge eigenstates [i.e., propagation with Eq. (24) implicitly assumes that $\mathbf{C}_s^{\rm eig}(0)=0$]. The above derivation is applicable to systems where there are $n>2$ localized states in the bridge HOMO–LUMO gap. In this case the superexchange electron-transfer probabilities between these states are approximated by solving an effective n-state TDSE analogous to Eq. (50).[51]

A. Numerical tests of the approximations

To test numerically the assumptions made in the derivation of the two-state TDSE, Eqs. (39)–(42) are put into a more compact form. The following quantities are defined:

$$f_1(t)=|\Psi_{A+}(t)|^2+|\Psi_{D+}(t)|^2+|\Psi_{A-}(t)|^2 +|\Psi_{D-}(t)|^2,$$
$$f_2(t)=\sum_{m\neq\pm}|\Psi_{Am}(t)|^2+|\Psi_{Dm}(t)|^2, \quad (52)$$

where $f_1(t)$ measures, at each time t, the total contribution of $\mathbf{\Psi}_+(t)$ and $\mathbf{\Psi}_-(t)$ to $\langle\phi_D(t)|\phi_D(t)\rangle$ and $\langle\phi_A(t)|\phi_A(t)\rangle$ (i.e., to the static ϕ_D and ϕ_A populations). $f_2(t)=\Sigma_{m\neq\pm}|\Psi_{Dm}(t)|^2+|\Psi_{Am}(t)|^2$ is an analogous (collective) measure for all remaining eigenstates $\mathbf{\Psi}_{m\neq\pm}(t)$. If there exist only two gap eigenstates $\mathbf{\Psi}_\pm$ and two gap-localized states ϕ_D, ϕ_A such that Eqs. (39)–(42) are valid, then $f_1(t)\gg f_2(t)$.

To differentiate between the situation described by Eqs. (39)–(40) and that described by Eqs. (41)–(42), we consider the quantities

$$g_1(t)=|\Psi_{D+}(t)|^2|\Psi_{A+}(t)|^2+|\Psi_{D-}(t)|^2|\Psi_{A-}(t)|^2,$$
$$g_2(t)=\sum_{m\neq\pm}|\Psi_{Dm}(t)|^2|\Psi_{Am}(t)|^2, \quad (53)$$

where $g_1(t)$ measures whether, at any time t, $\mathbf{\Psi}_+(t)$ (or $\mathbf{\Psi}_-(t)$) has a large ϕ_D component and simultaneously a large ϕ_A component. The maximum value of g_1 is realized for a purely two-state system at resonance, i.e., for $\hat{H}=\epsilon_D|\phi_D\rangle\langle\phi_D|+\epsilon_A|\phi_A\rangle\langle\phi_A|+(v_{DA}|\phi_D\rangle\langle\phi_A|+\text{h.c.})$ with $\epsilon_D=\epsilon_A$. In this case $|\Psi_\pm\rangle=(1/\sqrt{2})|\phi_D\rangle\pm(1/\sqrt{2})|\phi_A\rangle$ and $g_1=g_1^{\max}=0.5$. $g_2(t)$ is similar to $g_1(t)$, defined collectively for all remaining eigenstates $\mathbf{\Psi}_{m\neq\pm}(t)$. When Eqs. (41) and (42) are valid (a necessary condition for the validity of the two-state TDSE), $g_1(t)\gg g_2(t)$.

The quantities $f_{1(2)}(t)$, $g_{1(2)}(t)$, $\rho_{m\pm}(t)$, and $|C_\pm^{\text{eig}}(t)|^2$ are studied as a function of $\langle\epsilon_D\rangle$ and $\langle\epsilon_A\rangle$ at fixed $\phi_D-\phi_A$ separation, and are related to the performance of $P_{DA}^{2s}(t)$ as an approximation for $P_{DA}(t)$. The system of Fig. 4(a) is used as reference because it describes a case where $P_{DA}^{2s}(t)$ is a very good approximation to $P_{DA}(t)$ at all times. Therefore, for this system, all assumptions made in the derivation of the two-state TDSE should also be valid at all times. The main assumptions involve Eqs. (41) and (42) [equivalent to $f_1(t)\gg f_2(t)$ and $g_1(t)\gg g_2(t)$], and Eq. (45).

Figures 6–9 all refer to the MD trajectory and $\phi_D-\phi_A$ pair of Fig. 4(a) (Met-121–Lys-122), with $\langle E_{\text{homo}}^{\text{bri}}\rangle\simeq-12$ eV and $\text{rms}\{\delta E_{\text{homo}}^{\text{bri}}\}\simeq0.1$ eV. In Figs. 6(a)–9(a) $\epsilon_D(0)=\epsilon_A(0)=-10$ eV and $\langle\epsilon_D\rangle\simeq\langle\epsilon_A\rangle\simeq-10$ eV. This is the reference system of Fig. 4(a), and $\langle\epsilon_D\rangle$ and $\langle\epsilon_A\rangle$ are inside the bridge HOMO–LUMO gap. In Figs. 6(b)–9(b) $\epsilon_D(0)=\epsilon_A(0)=-12$ eV and $\langle\epsilon_D\rangle\simeq\langle\epsilon_A\rangle\simeq-12$ eV (at the HOMO edge of the gap). Finally, in Figs. 6(c)–9(c), $\langle\epsilon_D\rangle$ and $\langle\epsilon_A\rangle$ are inside the bridge eigenspectrum with $\epsilon_D(0)=\epsilon_A(0)=-13$ eV and $\langle\epsilon_D\rangle\simeq\langle\epsilon_A\rangle\simeq-13$ eV. The average ϕ_D and ϕ_A energies in these cases are changed by reducing the time-independent ϵ in $\epsilon_A(t)=\mathbf{F}_{AA}(t)+\epsilon$ and $\epsilon_A(t)=\mathbf{F}_{AA}(t)+\epsilon$ (Sec. II).

Figure 6 compares the exact electron-transfer probability $P_{DA}(t)$ and the approximate two-state probability $P_{DA}^{2s}(t)$ for cases (a)–(c). When $\langle\epsilon_D\rangle$ and $\langle\epsilon_A\rangle$ are inside the bridge HOMO–LUMO gap or even at the edge of the gap [Figs. 5(a) and 5(b)], $P_{DA}^{2s}(t)$ is a good approximation to $P_{DA}(t)$.

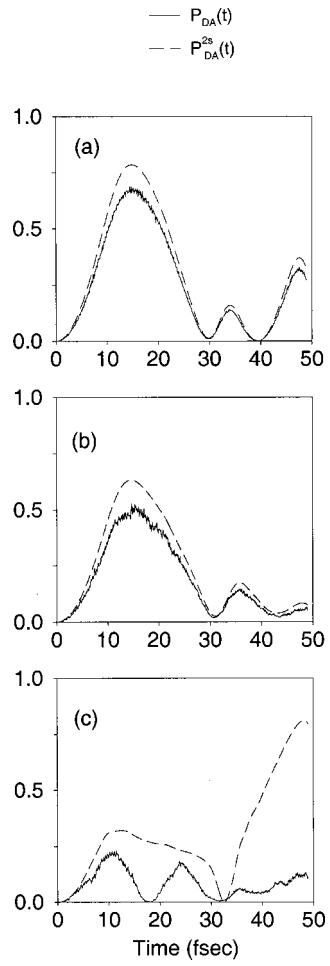

FIG. 6. Initial (50 fs) dynamics of the exact $P_{DA}(t)$ [Eq. (19)] and the approximate $P_{DA}^{2s}(t)$ for the $\phi_D-\phi_A$ pair Met-121–Lys-122 and for different values of $\langle\epsilon_D\rangle$ and $\langle\epsilon_A\rangle$. The values of $\langle\epsilon_D\rangle\simeq\langle\epsilon_A\rangle$ are: (a) -10 eV; (b) -12 eV; (c) -13 eV. In all cases (a)–(c) $\langle E_{\text{homo}}^{\text{bri}}\rangle\simeq-12$ eV, $\text{rms}\{\delta E_{\text{homo}}^{\text{bri}}\}\simeq0.1$ eV, and $\epsilon_D(0)=\epsilon_A(0)$.

When $\langle\epsilon_D\rangle$ and $\langle\epsilon_A\rangle$ enter the bridge eigenspectrum [Fig. 6(c)], $P_{DA}^{2s}(t)$ ceases to be a good approximation to $P_{DA}(t)$ after 10 fs. Figures 7(a)–7(c) show $f_1(t)$, $f_2(t)$ (left) and $g_1(t)$, $g_2(t)$ (right) for the systems in Figs. 6(a)–6(c). When $P_{DA}^{2s}(t)\simeq P_{DA}(t)$ [Figs. 6(a) and 6(b)], $f_1(t)\simeq1.8\gg f_2(t)\simeq0.2$, and $g_1(t)\gg g_2(t)\simeq5\times10^{-5}$ [Figs. 7(a) and 7(b)]. The two-state approximation is valid at all times because $g_1(t)$ is always large with respect to $g_2(t)$ [Eqs. (41) and (42) are satisfied]. Each eigenstate $\mathbf{\Psi}_+(t)$ and $\mathbf{\Psi}_-(t)$ used to compute $P_{DA}^{2s}(t)$ has simultaneously a large ϕ_D and a large ϕ_A component at all times, as assumed in the derivation of the two-state TDSE. In contrast, when $P_{DA}^{2s}(t)\neq P_{DA}(t)$ [Fig. 6(c)], $f_1(t)<f_2(t)$ and $g_1(t)\simeq g_2(t)$ at 10–20 fs and 30–40 fs [Fig. 7(c)]. During these time intervals Eqs. (39)–(42) are violated. The eigenstates that have the largest ϕ_D and ϕ_A components for the initial system conformation lose this property after 10 fs because there is strong mixing between ϕ_D, ϕ_A, and $\{\phi_i^{\text{br}}\}$. After 10 fs $P_{DA}^{2s}(t)$ deviates from $P_{DA}(t)$.

Figures 8(a)–8(c) are plots of $\max\{\rho_{m+}(t)\}$ (left) and $\max\{\rho_{m-}(t)\}$ (right) for the cases considered above [$\rho_{m\pm}(t)$ given in Eq. (45)]. When $P_{DA}^{2s}(t)\simeq P_{DA}(t)$ [Figs. 6(a) and

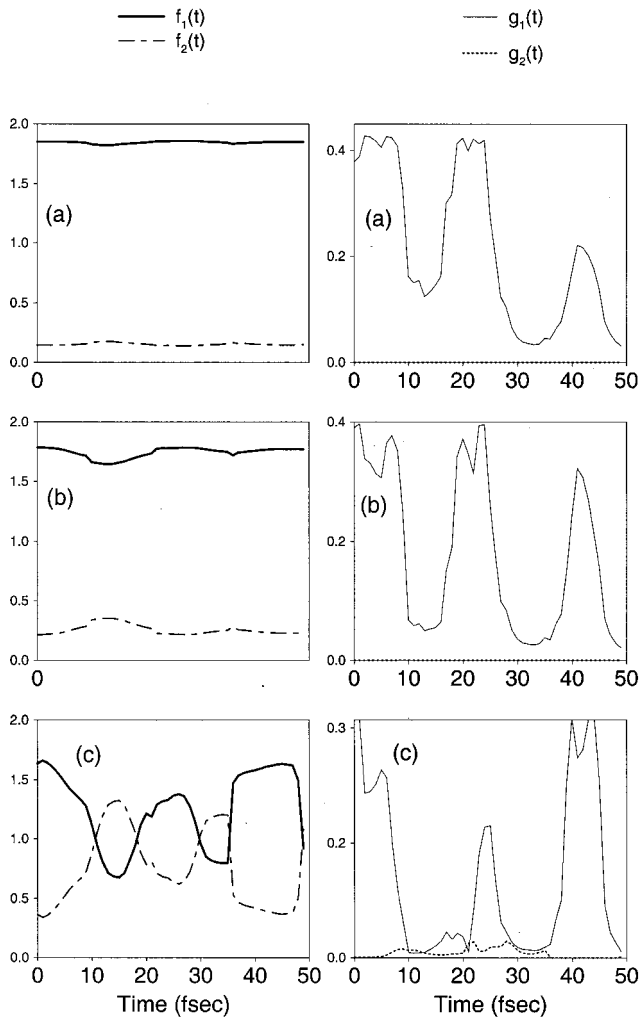

FIG. 7. $f_1(t)$ vs $f_2(t)$ [Eq. (52), left graph], and $g_1(t)$ vs $g_2(t)$ [Eq. (53), right graph] for the systems in Fig. 6. $\langle \epsilon_D \rangle \simeq \langle \epsilon_A \rangle$: -10 eV (a); -12 eV (b); -13 eV (c). For cases (a) and (b) $g_2(t)$ is negligible compared to $g_1(t)$ at all times.

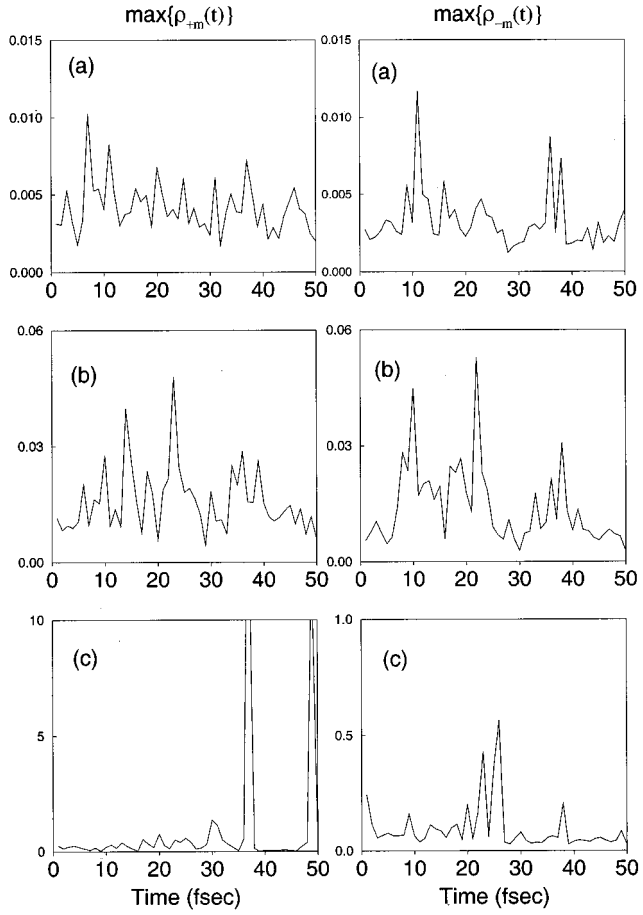

FIG. 8. Plot of $\max\{\rho_{+m}(t)\}$ (left graph) and $\max\{\rho_{-m}(t)\}$ (right graph) where $\rho_{m\pm}(t)$ is given in Eq. (45). The systems considered are identical to those in Fig. 6. $\langle \epsilon_D \rangle \simeq \langle \epsilon_A \rangle$: -10 eV (a); -12 eV (b); -13 eV (c).

6(b)], $\max\{\rho_{m\pm}(t)\} \sim 10^{-2} \ll 1$ [Figs. 8(a) and 8(b)]. This is consistent with the second assumption made in the derivation of the two-state TDSE [Eq. (45)]. When $P_{DA}^{2s}(t) \neq P_{DA}(t)$ [Fig. 6(c)], $\max\{\rho_{m\pm}(t)\} \sim 1$–$10$ [Fig. 8(c)] and Eq. (45) is violated. The elements $K_{\pm m}^{\mathrm{eig}}(t)$ that couple $\mathbf{\Psi}_{\pm}(t)$ to $\mathbf{\Psi}_{m\neq\pm}(t)$ become of the same order as (or greater than) $(E_m(t) - E_{\pm}(t))/\hbar$. $\langle \epsilon_D \rangle$ and $\langle \epsilon_A \rangle$ lie inside the bridge eigenspectrum and $\mathbf{\Psi}_{\pm}(t)$ are not energetically separated from the other $\mathbf{\Psi}_m(t)$.

Figures 9(a)–9(c) test the validity of Eqs. (43), (46), and (47). Two types of eigenstate probabilities are shown: (i) The exact $P_+(t) = |C_+^{\mathrm{eig}}(t)|^2$ (left) and $P_-(t) = |C_-^{\mathrm{eig}}(t)|^2$ (right) where $C_{\pm}^{\mathrm{eig}}(t)$ are computed from Eq. (32) [Eq. (44)]; (ii) Approximate $\tilde{P}_+(t) = |\tilde{C}_+^{\mathrm{eig}}(t)|^2$ (left, circles) and $\tilde{P}_-(t) = |\tilde{C}_-^{\mathrm{eig}}(t)|^2$ (right, circles) where $\tilde{C}_{\pm}^{\mathrm{eig}}(t)$ are computed using Eq. (46). When $\langle \epsilon_D \rangle$ and $\langle \epsilon_A \rangle$ are inside or at the edge the bridge HOMO–LUMO gap and $P_{DA}^{2s}(t) \simeq P_{DA}(t)$ [Figs. 6(a) and 6(b)], $|C_r^{\mathrm{eig}}(t)|^2 = P_+(t) + P_-(t) \simeq 0.8$–$0.9$ at all times and $|\mathbf{C}_r^{\mathrm{eig}}(t)|^2 \gg |\mathbf{C}_s^{\mathrm{eig}}(t)|^2$ [Figs. 9(a) and 9(b)]. Equations (43) and (47) are satisfied in these two cases. Furthermore, in Figs. 9(a) and 9(b) $P_{\pm}(t) \simeq \tilde{P}_{\pm}(t)$, indicating that $\mathbf{K}_{sr}^{\mathrm{eig}}$ ($\mathbf{K}_{rs}^{\mathrm{eig}}$) can be ignored in Eq. (44) [since $\max\{\rho_{m\pm}(t)\} \ll 1$ in Figs. 8(a) and 8(b)], giving rise to Eq. (46). In contrast, when $\langle \epsilon_D \rangle$ and $\langle \epsilon_A \rangle$ enter the bridge eigenspectrum and $P_{DA}^{2s}(t) \neq P_{DA}(t)$ [Fig. 6(c)], $|\mathbf{C}_r^{\mathrm{eig}}(t)|^2 = P_+(t) + P_-(t)$ decreases rapidly as a function of time (0.85 at $t=0$ and 0.45 at $t = 50$ fs), and $P_{\pm}(t) \neq \tilde{P}_{\pm}(t)$ [Fig. 9(c)]. The matrix elements $K_{\pm m}^{\mathrm{eig}}(t)$ become important [$\max\{\rho_{m\pm}(t)\} \sim 1$–$10$ in Fig. 8(c)], and they induce transitions between $\mathbf{\Psi}_{\pm}(t)$ and $\mathbf{\Psi}_{m\neq\pm}(t)$, causing loss of population from $|\mathbf{C}_r^{\mathrm{eig}}(t)|^2$ to $|\mathbf{C}_s^{\mathrm{eig}}(t)|^2$.

In Sec. III (Fig. 4) it was shown that $P_{DA}^{2s}(t)$ becomes a progressively worse approximation to $P_{DA}(t)$ (within a given time window) as the $\phi_D - \phi_A$ separation increases at constant $\langle \epsilon_D \rangle$ and $\langle \epsilon_A \rangle$. For all cases in Fig. 4 the MD trajectory and $\epsilon_D(t)/\epsilon_A(0)$ are identical [with $\epsilon_D(0) = \epsilon_A(0) = -10$ eV and $\langle \epsilon_D \rangle \simeq \langle \epsilon_A \rangle \simeq -10$ eV]. The discrepancy between $P_{DA}^{2s}(t)$ and $P_{DA}(t)$ for the larger $\phi_D - \phi_A$ separations arises from the slowing down (increased nonadiabaticity) of the gap-eigenstate (superexchange) contribution to $P_{DA}(t)$. As the gap-eigenstate contribution [approximated by $P_{DA}^{2s}(t)$] slows down, the contribution of the remaining eigenstates is revealed and it dominates the initial dynamics of $P_{DA}(t)$. Figures 10(a)–10(d) are plots of $g_1(t)$ and $g_2(t)$ [Eq. (53)] for the initial 200 fs of the systems in Fig. 4(a) ($\phi_D - \phi_A$: Met-121–Lys122); Fig. 4(d) (Met-121–Leu-125); and Fig. 4(e) (Met-121–Thr-126). In all three cases $f_1(t)$

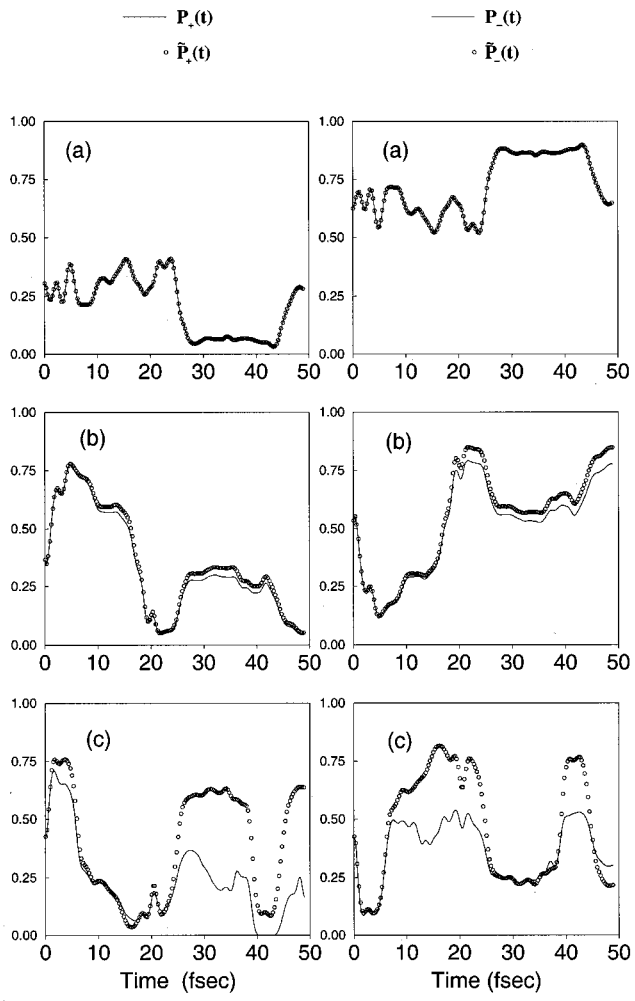

FIG. 9. Exact $P_+(t)=|C_+^{\mathrm{eig}}(t)|^2$ (left graph, line) and $P_-(t)=|C_-^{\mathrm{eig}}(t)|^2$ (right graph, line), where $C_\pm^{\mathrm{eig}}(t)$ are computed from Eq. (32), vs approximate $\tilde{P}_+(t)=|\tilde{C}_+^{\mathrm{eig}}(t)|^2$ (left graph, circles) and $\tilde{P}_-(t)=|\tilde{C}_-^{\mathrm{eig}}(t)|^2$ (right graph, circles), where $\tilde{C}_\pm^{\mathrm{eig}}(t)$ are computed using Eq. (46). Graphs (a) to (c) correspond to the systems in Fig. 6. $\langle\epsilon_D\rangle\simeq\langle\epsilon_A\rangle$: -10 eV (a); -12 eV (b); -13 eV (c).

$\simeq 1.8$, $f_2(t)\simeq 0.2$, and $\rho_{m\pm}(t)\ll 1$ (since $\langle\epsilon_D\rangle\simeq\langle\epsilon_A\rangle$ lie in the bridge HOMO–LUMO gap). For the shortest $\phi_D-\phi_A$ separation where $P_{DA}^{2s}(t)\simeq P_{DA}(t)$ [Fig. 4(a)], $g_1(t)\gg g_2(t)$ throughout the 200 fs time interval [Figs. 10(a) and 10(b)]. This is the reference system considered previously. For the larger $\phi_D-\phi_A$ separations where $P_{DA}^{2s}(t)\neq P_{DA}(t)$ within 200 fs [Figs. 4(d) and 4(e)], $g_1(t)\ll g_2(t)$ most of the 200 fs and $g_2(t)\simeq 10^{-5}$ [Figs. 10(c) and 10(d)]. In these latter cases the first assumption made in the derivation of the TDSE [Eqs. (41), (42)] is not satisfied the majority of the time; $\mathbf{\Psi}_+(t)$ ($\mathbf{\Psi}_-(t)$) does not have a large ϕ_D component and a large ϕ_A component simultaneously. Rather, the situation is described by Eqs. (39) and (40), ϕ_D is more strongly coupled to the bridge than to ϕ_A (and vice versa). In Figs. 10(c) and 10(d) $g_1(t)\gg g_2(t)$ only during very short, isolated time intervals centered at the crossing times of the effective donor and acceptor energies (resonance regions). Only during these short intervals is the two-state TDSE used to compute $P_{DA}^{2s}(t)$ a valid description of the electron-transfer dynamics. During each interval $P_{DA}^{2s}(t)$ contributes an amount $\simeq(2\pi)^2\gamma_{\mathrm{LZ}}\ll 1$ to $P_{DA}(t)$ [Eq. (29)]. In this regime the contribution of $P_{DA}^{2s}(t)$ becomes significant at times greater than 200 fs (Sec. III).

V. DISCUSSION

In summary, to construct a two-state TDSE that is a valid description of the electron-transfer dynamics from ϕ_D to ϕ_A within a given time interval, there must exist two eigenstates of the system [$\mathbf{\Psi}_+(t)$ and $\mathbf{\Psi}_-(t)$] that satisfy the following properties: (i) both ϕ_D and ϕ_A components of $\mathbf{\Psi}_+(t)$ ($\mathbf{\Psi}_-(t)$) should be large compared to the other $\{\phi_i^{\mathrm{br}}\}$ components [$g_1(t)\gg g_2(t)$ in Eq. (53)]; (ii) transitions between $\mathbf{\Psi}_\pm(t)$ and $\mathbf{\Psi}_{m\neq\pm}(t)$ caused by $\langle\Psi_\pm(t)|d_t\Psi_m(t)\rangle$ elements should not be important [i.e., $\rho_{m\pm}(t)\ll 1$ in Eq. (45)]. These conditions must be satisfied throughout the time interval of interest such that the two-state TDSE can be constructed using $\mathbf{\Psi}_+(t)$ and $\mathbf{\Psi}_-(t)$ [Eq. (24)].

As shown in the previous section, the second condition is easy to satisfy in the tunneling regime because ϕ_D and ϕ_A lie in the bridge HOMO–LUMO gap. The first condition [equivalent to Eqs. (41), (42)] is satisfied at all times for strongly coupled electron transfer. For long-distance (weakly coupled) electron transfer it is valid only around isolated donor–acceptor crossing times for very short time intervals. Most of the time $g_1(t)\ll g_2(t)$ [equivalent to Eqs. (39) and (40)], and only one of the eigenstates $\mathbf{\Psi}_+(t)$ or $\mathbf{\Psi}_-(t)$ has a large ϕ_D component (the other having only a large ϕ_A component). In this case electron transfer takes place through two competing independent channels, the gap-eigenstate channel, which describes superexchange electron transfer, and a channel involving all other ''nongap'' eigenstates that have bridge character. This latter channel is the coherent through-bridge mechanism that was explained in terms of a three-state system in Sec. I. The relative contributions of the two mechanisms to the initial dynamics of $P_{DA}(t)$ depends on the degree of nonadiabaticity of the electron-transfer reaction and on the nature of the $\phi_D(0)$ state. For strongly nonadiabatic electron transfer the superexchange channel is very slow, making negligible contribution to the initial $P_{DA}(t)$ and allowing coherent through-bridge transfer to dominate. The initial state $|\phi_D(0)\rangle$ is relevant to the coherent through-bridge mechanism because it determines the initial population of nongap eigenstates. This population is nonzero because, in general, $|\phi_D(0)\rangle\neq|\Psi_\pm(0)\rangle$.

A. Estimating the relative contributions of the coherent through-bridge and superexchange mechanisms

From a practical point of view it is useful to know whether $P_{DA}^{2s}(t)$ is a good approximation to $P_{DA}(t)$ within a time interval without having to propagate the TDSE of the N-state system [to compute $P_{DA}(t)$ for a comparison]. In Figs. 10(c) and 10(d), where $P_{DA}(t)$ is determined within 200 fs by the coherent-through-bridge amplitude $\Sigma_{m\neq\pm}\Psi_{Am}(t)C_m^{\mathrm{eig}}(t)$, it is observed that $\langle g_2(t)\rangle\simeq\langle P_{DA}(t)\rangle$. Therefore, the time average of $g_2(t)$ in Eq. (53) measures the total contribution of nongap eigenstates to $P_{DA}(t)$ even though $g_2(t)$ is a static quantity (i.e., it is computed from the time-*independent* Schrödinger equation at

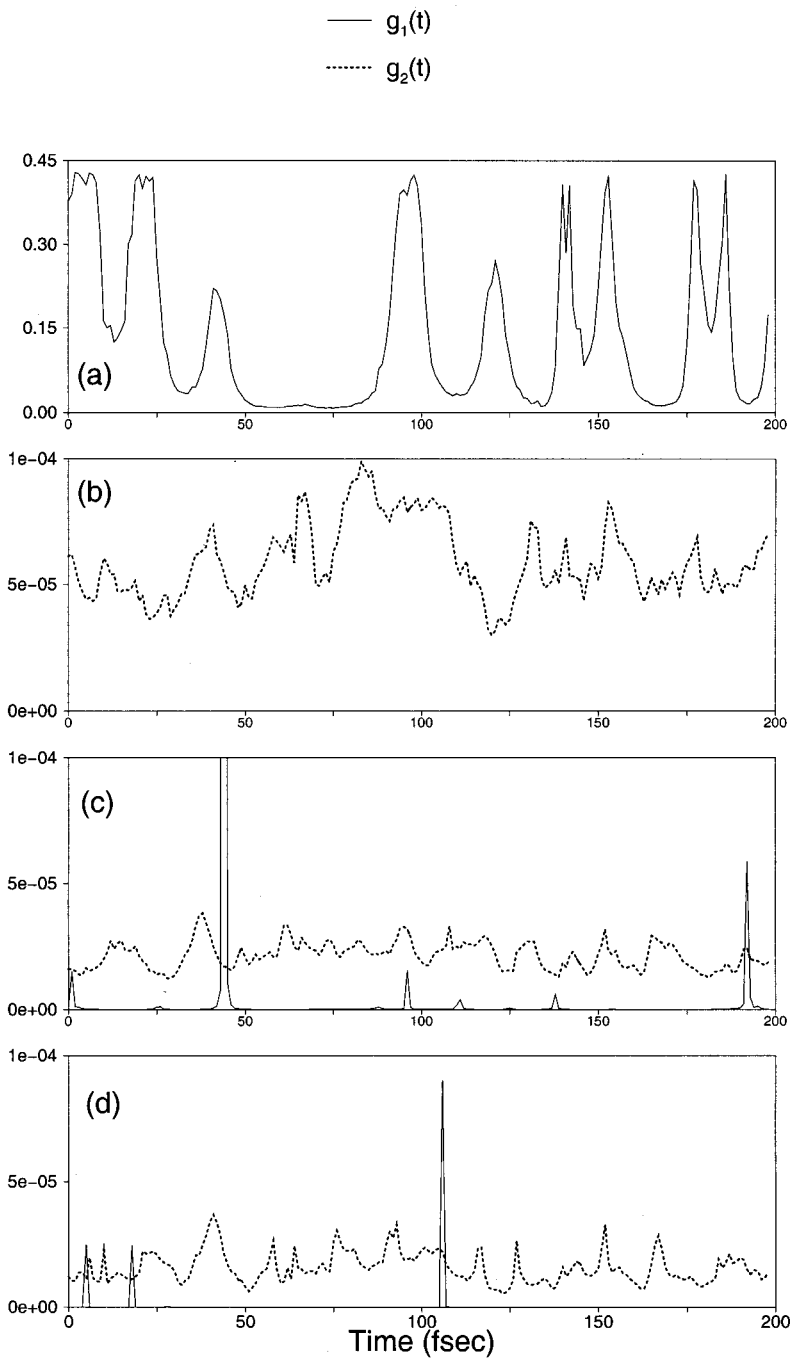

FIG. 10. (a) Plot of $g_1(t)$ for the initial 200 fs of the system in Fig. 4(a) ($\phi_D-\phi_A$ pair: Met-121–Lys-122). (b) Plot of $g_2(t)$ for the system in (a). (c) $g_1(t)$ and $g_2(t)$ for the initial 200 fs of the system in Fig. 4(d) ($\phi_D-\phi_A$ pair: Met-121–Leu-125). (d) $g_1(t)$ and $g_2(t)$ for the initial 200 fs of the system in Fig. 4(e) ($\phi_D-\phi_A$ pair: Met-121–Thr-126). In all cases the MD trajectory, $\epsilon_D(t)$, and $\epsilon_A(0)$ are identical [with $\epsilon_D(0)=\epsilon_A(0)=-10\,\mathrm{eV}$], and $\langle\epsilon_D\rangle\simeq\langle\epsilon_A\rangle\simeq-10\,\mathrm{eV}$. $g_1(t)$ and $g_2(t)$ are given in Eq. (53).

each t). This observation is generally true in the tunneling regime because, as shown in the derivation of the two-state TDSE, the total population of nongap eigenstates does not change with time (since transitions between them and the gap eigenstates are suppressed). It means that $\langle g_2(t)\rangle$ can be used to estimate the importance of the coherent through-bridge channel that competes with superexchange without calculating the exact $P_{DA}(t)$. For example, if within a time interval T of simulation $\langle g_2(t)\rangle_T \gg P_{DA}^{2s}(t)$, the superexchange contribution to the dynamics of $P_{DA}(t)$ is negligible within T. In this situation it is also possible to estimate the time $T^*>T$ needed for the superexchange channel to dominate. To this end, using Eq. (29) we set

$$\langle g_2(t)\rangle_{T^*}\simeq\max\{P_{DA}^{2s}(t)\}\simeq(2\pi)^2(N_c)_{T^*}(\gamma_{\mathrm{LZ}}^{(\mathrm{rms})})_{T^*}, \tag{54}$$

where the subscript T^* implies that N_c and $\gamma_{\mathrm{LZ}}^{(\mathrm{rms})}$ refer to (unknown) averages over the time interval T^*. In the left side of Eq. (54) $\langle g_2(t)\rangle_{T^*}\simeq\langle g_2(t)\rangle_T$ because $\langle g_2(t)\rangle$ remains approximately constant as a function of averaging time (e.g., for the systems in Figs. 10(b)–10(d) $\langle g_2(t)\rangle_{200\,\mathrm{fs}}\simeq\langle g_2(t)\rangle_{1\,\mathrm{ps}}$). This is expected to happen as long as $\epsilon_D(t)$ and $\epsilon_A(t)$ remain in the same region of the HOMO–LUMO gap (see the perturbative argument for the three-state system in Sec. I). Setting $T^*=mT$ we can solve for m in terms of known (computed) quantities by assuming that the statistics

of donor–acceptor crossings does not change for $T^*>T$. Then, in the right side of Eq. (54) $(N_c)_{T^*}\simeq m(N_c)_T$ and $(\gamma_{\mathrm{LZ}}^{(\mathrm{rms})})_{T^*}\simeq(\gamma_{\mathrm{LZ}}^{(\mathrm{rms})})_T$. Solving for m gives the amount of time needed for the superexchange mechanism to dominate, $T^*=mT$ where $m=\langle g_2(t)\rangle_T/(2\pi)^2(N_c)_T(\gamma_{\mathrm{LZ}}^{(\mathrm{rms})})_T$.

The results presented in this work are more relevant to single-molecule experiments because our calculations do not involve ensemble averaging. However, our main conclusions can be applicable to experiments that measure ensemble averages as long as there is not significant ensemble inhomogeneity in the system properties that determine the coherent through-bridge mechanism. These properties are: (a) The donor(acceptor) energetics with respect to the bridge (ϵ_D and ϵ_A must lie inside the bridge HOMO–LUMO gap for all systems in the ensemble); (b) The degree of nonadiabaticity of the reaction (electron transfer must be strongly nonadiabatic for all systems in the ensemble). To draw a conclusion about the mechanism of electron transfer, the amount of time needed for the superexchange mechanism to dominate (T^*) should be compared to the average time that the system spends in the crossing region between donor and acceptor free-energy surfaces (τ_{rel} in Fig. 3). If $T^*\gg\tau_{\mathrm{rel}}$ then the electron-transfer rate is not determined by superexchange dynamics, even though donor and acceptor are off-resonant to the bridge. In protein-aqueous environments, τ_{rel} can be as fast as $\sim 10^2$ fs[3,52] and within such time scales the superexchange component to the probability may be insignificant (Fig. 4). Therefore, the coherent through-bridge mechanism is plausible.

An experimental signature of the coherent through-bridge mechanism would be an independence of the rate to changes in the donor–acceptor separation for large separations. Furthermore, this behavior should persist at low temperatures because it arises from a coherent mechanism of transfer and has purely electronic origin. At low temperatures any independence of the rate to changes in donor–acceptor separation that is related to electron–bridge–phonon energy exchange is suppressed (see Ref. 20 for a review), and the coherent through-bridge mechanism should be discernible. Another important determinant of this mechanism, the degree of donor delocalization into the bridge, can also be estimated from experiments[53] (e.g., charge transfer bands and ESR).

B. Time-dependent superexchange pathways

In previous work[21] we described a time-dependent two-state approximation for electron transfer based on the Löwdin projection method, in order to formulate time-dependent superexchange pathways. The effective Hamiltonian used to propagate the two-state TDSE was

$$\mathbf{H}^{2s}(E_{\mathrm{tun}},t)\equiv\begin{pmatrix}\epsilon_D(t)+T_{DD}(t) & v_{DA}(t)+T_{DA}(t)\\ v_{AD}(t)+T_{AD}(t) & \epsilon_A(t)+{}_{AA}(t)\end{pmatrix}, \tag{55}$$

rather than the $\mathbf{H}^{2s}(t)$ in Eqs. (22) and (23). In $\mathbf{H}^{2s}(E_{\mathrm{tun}},t)$ $\epsilon_D(t)$ and $\epsilon_A(t)$ are the "bare" ϕ_D (ϕ_A) site energies and $v_{DA}(t)$ is the direct $D-A$ coupling [the elements of $\hat{H}_{DA}(t)$ in Eq. (9)]. The effective (bridge-mediated) matrix elements of $\mathbf{H}^{2s}(E_{\mathrm{tun}},t)$ are given by

$$T_{KL}(t)=\sum_{ij} v_{Ki}(t)G_{ij}^{\mathrm{br}}(E_{\mathrm{tun}}(t),t)v_{jL}(t),\quad K(L)=D,A. \tag{56}$$

$T_{KL}(t)$ contain the (energy-domain) bridge Green's function for a "static" bridge frozen at its conformation at time t, i.e.,

$$G_{ij}^{\mathrm{br}}(E_{\mathrm{tun}}(t),t)=\langle\phi_i^{\mathrm{br}}(t)|(E_{\mathrm{tun}}(t)-\hat{H}^{\mathrm{br}}(t))^{-1}|\phi_j^{\mathrm{br}}(t)\rangle, \tag{57}$$

where $\hat{H}_{\mathrm{br}}(t)$ is given in Eq. (9) and $E_{\mathrm{tun}}(t)$ is the (time-dependent) tunneling energy of the electron.

$T_{DA}(t)$ contains in G_{ij}^{br} all the through-bridge superexchange-pathway information at time t. An accurate time-dependent pathway description of $P_{DA}(t)$ requires that $P_{DA}^{2s}(t)$ [computed from $\mathbf{H}^{2s}(E_{\mathrm{tun}},t)$ in Eq. (56)] be a good approximant to $P_{DA}(t)$. In Ref. 21 an optimum (good approximate) $P_{DA}^{2s}(t)$ was achieved by varying E_{tun} as a function of time. This observation can be understood in light of the more general two-state approximation described in Sec. II. $\mathbf{H}^{2s}(t)$ in Eqs. (22) and (23) is nonperturbative in the donor–bridge [$v_{Di}(t)$] and acceptor–bridge [$v_{Aj}(t)$] couplings because its matrix elements $H_{KL}^{2s}(t)$ are derived from the instantaneous gap eigenstates and eigenenergies of the entire donor–bridge–acceptor system. In contrast, the $T_{KL}(t)$ matrix elements of $\mathbf{H}^{2s}(E_{\mathrm{tun}},t)$ in Eq. (56) are perturbative in the donor–bridge and acceptor–bridge couplings. Therefore, each $H_{KL}^{2s}(t)$ is more accurate than its $T_{KL}(t)$ counterpart, and $P_{DA}^{2s}(t)$ computed from $\mathbf{H}^{2s}(t)$ in Eqs. (22) and (23) can be thought of as the optimal two-state approximation for the description of a superexchange $P_{DA}(t)$. If the same $P_{DA}(t)$ is approximated by computing $P_{DA}^{2s}(t)$ from $\mathbf{H}^{2s}(E_{\mathrm{tun}},t)$, then in order to obtain $P_{DA}^{2s}(t)\simeq P_{DA}(t)$ the $T_{KL}(t)$ matrix elements must be adjusted as a function of time to reproduce the $H_{KL}^{2s}(t)$ elements. At any t the relations

$$T_{AA}(t)=H_{AA}^{2s}(t)-\epsilon_A(t),\quad T_{DD}(t)=H_{DD}^{2s}(t)-\epsilon_D(t),$$

and

$$T_{DA}(t)=H_{DA}^{2s}(t)-v_{DA}(t) \tag{58}$$

should be satisfied, and this is possible only by adjuting E_{tun} in $T_{KL}(t)$ [the only free parameter in Eq. (58)]. The conclusion is that an accurate time-dependent tunneling-pathway analysis of electron transfer in the context of the Löwdin projection method [Eqs. (56), (57)] requires a time-dependent E_{tun}. The diagonalization procedure [Eqs. (22), (23)] provides the reference calculation for computing correct tunneling energies.

1. The interpretation of pathways and the relevance of the crossing dynamics between effective donor and acceptor states

In a situation where $P_{DA}(t)$ is superexchange [$P_{DA}(t)\simeq P_{DA}^{2s}(t)$], the time-dependent superexchange matrix element between ϕ_D and ϕ_A is central to the description of the electron-transfer dynamics. The time dependence of $H_{DA}^{2s}(t)$ [or equivalently of the optimized $T_{DA}^{2s}(t)$] reflects the influ-

ence of protein motion on the coupling between ϕ_D and ϕ_A. The analysis of the overall effect of H_{DA}^{2s} fluctuations on the rate and the interpretation of superexchange pathways depends on the crossing dynamics between the effective donor and acceptor states.

As shown in Sec. III, in the case of strongly nonadiabatic electron transfer, $P_{DA}(t)$ can be approximated as a sum of independent electron-transfer probabilities $(2\pi)^2\gamma(t_i^*)$ at the crossing times $\{t_i^*\}$ where $H_{DD}^{2s}(t_i^*)=H_{AA}^{2s}(t_i^*)$. The Landau–Zener parameter $\gamma(t_i^*)$ contains $|H_{DA}^{2s}(t_i^*)|^2$. Therefore, the time dependence of $H_{DA}^{2s}(t)$ is ''sampled'' at the discrete $\{t_i^*\}$ and the relevant values of the tunneling matrix element are the set $\{H_{DA}^{2s}(t_i^*)\}$. To understand this limit we write $\gamma_{\mathrm{LZ}}(t_i^*)=\tau_{\mathrm{LZ}}(t_i^*)/\tau_{\mathrm{Rabi}}(t_i^*)$, where $\tau_{\mathrm{LZ}}(t_i^*)=|H_{DA}^{2s}(t_i^*)|/|d_t[H_{DD}^{2s}(t_i^*)-H_{AA}^{2s}(t_i^*)]|$ is the Landau–Zener time and $\tau_{\mathrm{Rabi}}(t_i^*)=h/|H_{DA}^{2s}(t_i^*)|$ is the Rabi time. $\tau_{\mathrm{LZ}}(t_i^*)$ is the time interval around each t_i^* during which the effective donor and acceptor states are quasiresonant ($|H_{DA}^{2s}|<|H_{DD}^{2s}-H_{AA}^{2s}|$) and the electron-transfer transition is possible. If the minimum time scale of $H_{DA}^{2s}(t)$ fluctuations is greater than the average τ_{LZ}, then within the τ_{LZ} region surrounding each t_i^* $H_{DA}^{2s}(t)$ can be replaced by its value at t_i^* [$H_{DA}^{2s}(t)\simeq H_{DA}^{2s}(t_i^*)$]. In this case the fluctuations of $H_{DA}^{2s}(t)$ are sampled by donor and acceptor only at the crossing times. The importance of each $H_{DA}^{2s}(t_i^*)$ to the overall rate is determined by the product of the probability $(2\pi)^2\gamma(t_i^*)$ with the probability of finding the system at the particular protein conformation at t_i^*. Therefore, the effect of matrix-element fluctuations can be analyzed using statistical arguments. For example, it is meaningful to compute the average of $|H_{DA}^{2s}|^2$ over the set of discrete crossing times. Similarly, in structure-function analysis of the tunneling matrix element, it is only necessary to consider the ''snapshots'' of the time-dependent pathways at the crossing times.

In the case of more strongly coupled (more adiabatic) electron transfer [e.g., Figs. 4(a) and 10(a)–10(b)], the superexchange contribution to $P_{DA}(t)$ cannot be described by a sum of $(2\pi)^2\gamma(t_i^*)$. The average time interval of donor–acceptor resonance [width of $g_1(t)$ peaks in Fig. 10] increases with increasing adiabaticity, and it may become longer than the shortest time scale of fluctuation of $H_{DA}^{2s}(t)$. When this happens the full time dependence of $H_{DA}^{2s}(t)$ within each resonance interval [not just $H_{DA}^{2s}(t_i^*)$] is relevant to the electron-transfer dynamics, and at different times within the interval the $H_{DA}^{2s}(t)$ interfere. The two-state TDSE must be used [rather than $(2\pi)^2\gamma(t_i^*)$] to obtain the superexchange contribution to $P_{DA}(t)$ that takes into account this coherence. The statistical analysis of matrix-element fluctuations and of superexchange pathways mentioned above is not valid.[54] In this limit of ''fast'' $H_{DA}^{2s}(t)$ fluctuations $\tau_{\mathrm{LZ}}(t_i^*)$ is not a good measure of the length of a resonance region because a single value of $H_{DA}^{2s}(t)$ [such as $H_{DA}^{2s}(t_i^*)$] is irrelevant. A better measure is the width of the $g_1(t)$ peak [Eq. (53) and Fig. 10] that is computed by use of the time-independent Schrödinger equation. In a simulation, to decide whether a statistical or a coherent analysis of the time-dependent matrix element (and of pathways) should be used, the average width of $g_1(t)$ peaks should be compared to the shortest time scale of fluctuations in $H_{DA}^{2s}(t)$.

ACKNOWLEDGMENT

This work is supported by the University of Cyprus research program: ''From Strong Interactions to Molecular Recognition: Theoretical and Computational Studies.''

APPENDIX: PARTITIONING IN THE LOCALIZED-STATE AND EIGENSTATE SPACES

The basis set of localized orbitals $\{\phi_i\}$ is partitioned into the relevant subspace of the ϕ_D and ϕ_A orbitals (denoted p), and the subspace of bridge ϕ_i^{br} orbitals (denoted q). Therefore, in Eq. (18)

$$\mathbf{C}^{\mathrm{loc}}(t)=\begin{pmatrix}\mathbf{C}_p^{\mathrm{loc}}(t)\\ \mathbf{C}_q^{\mathrm{loc}}(t)\end{pmatrix},$$

$$\text{where}\quad \mathbf{C}_p^{\mathrm{loc}}(t)=\begin{pmatrix}C_D^{\mathrm{loc}}(t)\\ C_A^{\mathrm{loc}}(t)\end{pmatrix}$$

$$\text{and}\quad \mathbf{C}_q^{\mathrm{loc}}(t)=\begin{pmatrix}\cdot\\ C_i^{\mathrm{loc}}(t)\\ \cdot\end{pmatrix}\quad (i\neq D,A). \tag{A1}$$

Furthermore, in Eqs. (16) and (17)

$$\mathbf{H}^{\mathrm{loc}}=\begin{pmatrix}\mathbf{H}_{pp}^{\mathrm{loc}} & \mathbf{H}_{pq}^{\mathrm{loc}}\\ \mathbf{H}_{qp}^{\mathrm{loc}} & \mathbf{H}_{qq}^{\mathrm{loc}}\end{pmatrix},\quad \mathbf{K}^{\mathrm{loc}}=\begin{pmatrix}\mathbf{K}_{pp}^{\mathrm{loc}} & \mathbf{K}_{pq}^{\mathrm{loc}}\\ \mathbf{K}_{qp}^{\mathrm{loc}} & \mathbf{K}_{qq}^{\mathrm{loc}}\end{pmatrix}. \tag{A2}$$

$\mathbf{H}_{pp}^{\mathrm{loc}}$, $\mathbf{H}_{qq}^{\mathrm{loc}}$, and $\mathbf{H}_{pq}^{\mathrm{loc}}(\mathbf{H}_{qp}^{\mathrm{loc}})$ are the Hamiltonian submatrices with the elements of $\hat{H}_{DA}$, $\hat{H}_{\mathrm{br}}$, and $\hat{H}_{DA-\mathrm{br}}$, respectively [Eq. (9)]. A summary of the above notation is given in Table I.

The basis set of instantaneous eigenstates $|\Psi_m\rangle$ is partitioned into the relevant subspace (r) of the gap eigenstates $|\Psi_+\rangle$ and $|\Psi_-\rangle$ that are used in the two-state approximation, and the subspace (s) of all remaining eigenstates. Therefore, in Eq. (31)

$$\mathbf{C}^{\mathrm{eig}}(t)=\begin{pmatrix}\mathbf{C}_r^{\mathrm{eig}}(t)\\ \mathbf{C}_s^{\mathrm{eig}}(t)\end{pmatrix},$$

$$\text{where}\quad \mathbf{C}_r^{\mathrm{eig}}(t)=\begin{pmatrix}C_+^{\mathrm{eig}}(t)\\ C_-^{\mathrm{eig}}(t)\end{pmatrix}$$

$$\text{and}\quad \mathbf{C}_s^{\mathrm{eig}}(t)=\begin{pmatrix}\cdot\\ C_m^{\mathrm{eig}}(t)\\ \cdot\end{pmatrix}\quad (m\neq\pm), \tag{A3}$$

and in Eqs. (32) and (33)

$$\mathbf{H}^{\mathrm{eig}}=\begin{pmatrix}\mathbf{H}_{rr}^{\mathrm{eig}} & \mathbf{H}_{rs}^{\mathrm{eig}}\\ \mathbf{H}_{sr}^{\mathrm{eig}} & \mathbf{H}_{ss}^{\mathrm{eig}}\end{pmatrix},\quad \mathbf{K}^{\mathrm{eig}}=\begin{pmatrix}\mathbf{K}_{rr}^{\mathrm{eig}} & \mathbf{K}_{rs}^{\mathrm{eig}}\\ \mathbf{K}_{sr}^{\mathrm{eig}} & \mathbf{K}_{ss}^{\mathrm{eig}}\end{pmatrix}. \tag{A4}$$

Since $\mathbf{H}^{\mathrm{eig}}$ is diagonal, $\mathbf{H}_{rs}^{\mathrm{eig}}=\mathbf{H}_{sr}^{\mathrm{eig}}=0$ and $\mathbf{H}_{rr}^{\mathrm{eig}}$, $\mathbf{H}_{ss}^{\mathrm{eig}}$ are the 2×2 and $(N-2)\times(N-2)$ diagonal submatrices with elements E_+, E_- and E_m $(m\neq\pm)$, respectively. The above notation is summarized in Table II.

For the mth eigenvector $\mathbf{\Psi}_m(t)$ [Eq. (21)], the partitioning of the localized basis set leads to

$$\boldsymbol{\Psi}_m(t)=\begin{pmatrix}\boldsymbol{\Psi}_{pm}(t)\\ \boldsymbol{\Psi}_{qm}(t)\end{pmatrix},$$

$$\text{where}\quad \boldsymbol{\Psi}_{pm}(t)=\begin{pmatrix}\Psi_{Dm}(t)\\ \Psi_{Am}(t)\end{pmatrix}$$

$$\text{and}\quad \boldsymbol{\Psi}_{qm}(t)=\begin{pmatrix}\cdot\\ \Psi_{im}(t)\\ \cdot\end{pmatrix}\quad (i\neq D,A). \tag{A5}$$

For the eigenvector matrix $\boldsymbol{\Psi}(t)$ [Eq. (30)], the combination of Eq. (A5) above with the partitioning of the eigenvector space gives

$$\boldsymbol{\Psi}(t)=\begin{pmatrix}\boldsymbol{\Psi}_{p+} & \boldsymbol{\Psi}_{p-} & \cdot\cdot\boldsymbol{\Psi}_{pm}\cdot\cdot\\ \boldsymbol{\Psi}_{q+} & \boldsymbol{\Psi}_{q-} & \cdot\cdot\boldsymbol{\Psi}_{qm}\cdot\cdot\end{pmatrix}=\begin{pmatrix}\boldsymbol{\Psi}_{pr} & \boldsymbol{\Psi}_{ps}\\ \boldsymbol{\Psi}_{qr} & \boldsymbol{\Psi}_{qs}\end{pmatrix} \tag{A6}$$

(Table III). For example,

$$\boldsymbol{\Psi}_{p+}=\begin{pmatrix}\Psi_{D+}\\ \Psi_{A+}\end{pmatrix}\quad \text{and}\quad \boldsymbol{\Psi}_{q+}=\begin{pmatrix}\cdot\\ \Psi_{i+}\\ \cdot\end{pmatrix}\quad (i\neq D,A).$$

[1] R. A. Marcus and N. Sutin, Biochim. Biophys. Acta **811**, 265 (1987).
[2] M. D. Newton, Chem. Rev. **91**, 767 (1991).
[3] *Electron Transfer—from Isolated Molecules to Biomolecules*, edited by J. Jortner and M. Bixon, Advances in Chemical Physics **106**, 107 (1999).
[4] A. M. Kuznetsov and H. Ulstrup, *Electron Transfer in Chemistry and Biology* (Wiley, Chichester, 1988).
[5] M. D. Newton, in *Electron Transfer in Chemistry*, edited by V. Balzani, P. Piotrowiak, and M. A. J. Rodgers (Wiley-VCH, Weinheim, 2001), Vol. 1, pp. 3–63.
[6] D. N. Beratan, J. N. Betts, and J. N. Onuchic, Science **252**, 1285 (1991).
[7] S. S. Skourtis and D. N. Beratan, in *Advances in Chemical Physics*, edited by J. Jortner and M. Bixon, **106**, 377 (1999).
[8] J. R. Reimers and N. S. Hush, J. Phys. Chem. **95**, 9773 (1991).
[9] R. J. Cave and M. D. Newton, J. Chem. Phys. **106**, 9213 (1997).
[10] D. N. Beratan and J. J. Hopfield, J. Chem. Phys. **81**, 5753 (1984).
[11] J. N. Onuchic and A. A. S. Da Gamma, Theor. Chim. Acta **69**, 89 (1986); J. Am. Chem. Soc. **111**, 1315 (1989).
[12] A. M. Kuznetsov, M. D. Vigdorovich, and J. Ulstrup, Chem. Phys. **176**, 539 (1993).
[13] J. Tang, J. Chem. Phys. **98**, 6263 (1993).
[14] I. A. Goychuk, E. G. Petrov, and V. May, J. Chem. Phys. **103**, 4937 (1995).
[15] J. Wolfgang, S. Risser, S. Priyadarshy, and D. N. Beratan, J. Phys. Chem. B **101**, 2986 (1997).
[16] E. S. Medvedev and A. A. Stuchebrukhov, J. Chem. Phys. **107**, 3821 (1997).
[17] V. S. Pande and J. N. Onuchic, Phys. Rev. Lett. **78**, 146 (1997).
[18] L. W. Ungar, M. D. Newton, and G. A. Voth, J. Phys. Chem. B **103**, 7367 (1999).
[19] I. A. Balabin and J. N. Onuchic, Science **290**, 114 (2000).
[20] S. S. Skourtis and D. N. Beratan, in *Electron Transfer in Chemistry*, edited by V. Balzani, P. Piotrowiak, and M. A. J. Rodgers (Wiley-VCH, Weinheim, 2001), Vol. 1, pp. 109–125.
[21] Q. Xie, G. Archontis, and S. S. Skourtis, Chem. Phys. Lett. **312**, 237 (1999).
[22] A. Okada, V. Chernyak, and S. Mukamel, J. Phys. Chem. A **102**, 1241 (1998).
[23] J. Jortner, M. Bixon, T. Langenbacher, and M. E. Michel-Beyerle, Proc. Natl. Acad. Sci. U.S.A. **95**, 51 (1998).
[24] D. Segal, A. Nitzan, W. B. Davis, M. R. Wasielewski, and M. A. Ratner, J. Phys. Chem. B **104**, 3817 (2000).
[25] *Molecular Electronics*, edited by J. Jortner and M. Ratner (Blackwell Scientific, Oxford, 1997).
[26] H. Sumi and T. Kakitani, Chem. Phys. Lett. **252**, 85 (1996).
[27] E. P. Friis, Y. I. Kharkhats, A. M. Kuznetsov, and J. Ulstrup, J. Phys. Chem. A **102**, 7851 (1998).
[28] U. Peskin, A. Edlund, L. Bar-On, M. Galperin, and A. Nitzan, J. Chem. Phys. **111**, 7558 (1999).
[29] E. N. Baker, J. Mol. Biol. **203**, 1071 (1988).
[30] H. Frauenfelder and P. G. Wolynes, Science **229**, 337 (1985).
[31] G. A. Jones, B. K. Carpenter, and M. N. Paddon-Row, J. Am. Chem. Soc. **120**, 5499 (1998).
[32] J. J. Regan, A. J. Di Bilio, R. Langen, L. K. Skov, J. R. Winkler, H. B. Gray, and J. N. Onuchic, Chem. Biol. **2**, 489 (1995).
[33] A. Mackerell, D. Bashford, M. Bellott *et al.*, J. Phys. Chem. B **102**, 3586 (1998).
[34] W. L. Jorgensen, J. Chandrasekhar, J. D. Madura, R. W. Impey, and M. L. Klein, J. Chem. Phys. **79**, 926 (1983).
[35] N. F. Scherer, L. W. Ungar, and G. A. Voth. Biophys. J. **72**, 5 (1997).
[36] R. Stote, D. States, and M. Karplus. J. Chim. Phys. (Paris) **88**, 2419 (1991).
[37] C. Brooks and M. Karplus, J. Mol. Biol. **208**, 159 (1989).
[38] C. Brooks and M. Karplus, J. Chem. Phys. **79**, 6312 (1984).
[39] J. P. Ryckaert, G. Ciccotti, and H. J. C. Berendsen, J. Comput. Phys. **23**, 327 (1977).
[40] J. A. Pople and D. L. Beveridge, *Approximate Molecular Orbital Theory* (McGraw-Hill, New York, 1970).
[41] A. E. Reed, L. A. Curtiss, and F. Weinhold, Chem. Rev. **88**, 899 (1988).
[42] F. Weinhold, QCPE Program No. 408.
[43] M.-H Whangbo, M. Evain, T. Hughbanks, M. Kertesz, S. Wijeyesekera, C. Wilker, C. Zheng, and R. Hoffman, QCPE Program No. 571.
[44] S. S. Skourtis and J. N. Onuchic, Chem. Phys. Lett. **209**, 171 (1993).
[45] S. S. Skourtis, D. N. Beratan, and J. N. Onuchic, Chem. Phys. **176**, 501 (1993).
[46] S. S. Skourtis and S. Mukamel, Chem. Phys. **197**, 367 (1995).
[47] Alternatively, $\Psi_{D-}(t)$ and $\Psi_{A-}(t)$ could be used in Eqs. (22), (23).
[48] $\langle\ \rangle$ denotes a time average over an interval of 1 ps unless the time interval is specified by $\langle\ \rangle_T$.
[49] Ignoring the second term in Eq. (38) gives $i\hbar(d/dt)\mathbf{C}_p^{\mathrm{loc}}\simeq[\boldsymbol{\Psi}_{pr}\mathbf{H}_{rr}^{\mathrm{eig}}-i\hbar(\mathbf{K}^{\mathrm{loc}}\boldsymbol{\Psi})_{pr}]\mathbf{C}_r^{\mathrm{eig}}$. As discussed in Sec. II, in the context of the CNDO approximation the matrix $\mathbf{K}^{\mathrm{loc}}$ is not included in the computations involving the *N*-state TDSE in the localized basis [Eq. (16)]. Therefore, the term $(\mathbf{K}^{\mathrm{loc}}\boldsymbol{\Psi})_{pr}$ in the equation above should be ignored, giving Eq. (48). In general $\mathbf{K}^{\mathrm{loc}}$ has zero diagonal elements and its off-diagonal elements $\langle\phi_i|d_t\phi_j\rangle$ decay very fast with distance (since they depend on the overlap between localized states). Therefore, the effect of $\mathbf{K}^{\mathrm{loc}}$ on the electron transfer dynamics is negligible (Ref. 21).
[50] $\boldsymbol{\Psi}_{pr}(t)=(\boldsymbol{\Psi}_{p+}(t),\boldsymbol{\Psi}_{p-}(t))$, where $\boldsymbol{\Psi}_{p+}=\binom{\Psi_{D+}(t)}{\Psi_{A+}(t)}$ and $\boldsymbol{\Psi}_{p-}=\binom{\Psi_{D-}(t)}{\Psi_{A-}(t)}$. Equations (41) and (42) imply that $|\boldsymbol{\Psi}_{p+}(t)|^2\simeq|\boldsymbol{\Psi}_{p-}(t)|^2\simeq 1$ and $\boldsymbol{\Psi}_{p+}^T(t)\boldsymbol{\Psi}_{p-}(t)\simeq 0$. Therefore, $\boldsymbol{\Psi}_{pr}(t)\simeq\boldsymbol{\Psi}_{pr}^{\mathrm{un}}(t)=(\boldsymbol{\Psi}_{p+}^{\mathrm{orth}}(t),\boldsymbol{\Psi}_{p-}^{\mathrm{orth}}(t))$, where $\boldsymbol{\Psi}_{p+}^{\mathrm{orth}}(t)$ and $\boldsymbol{\Psi}_{p-}^{\mathrm{orth}}(t)$ are orthonormal forms of $\boldsymbol{\Psi}_{p+}(t)$ and $\boldsymbol{\Psi}_{p-}(t)$.
[51] In a situation where *n* localized donor/acceptor states lie in the bridge HOMO–LUMO gap ($N>n>2$), there will be an equal number of gap eigenstates. If *p* denotes the subspace of the *n* donor/acceptor states and *r* the subspace of the *n* gap eigenstates, the derivation of Sec. IV leads to an effective *n*-state TDSE and the necessary conditions for this reduction are *n*-state generalizations of the conditions discussed in Sec. IV.
[52] X. J. Jordanides, M. J. Lang, X. Song, and G. R. Fleming, J. Phys. Chem. **103**, 7995 (1999).
[53] R. D. Cannon, *Electron Transfer Reactions* (Butterworths, London, 1980).
[54] However, it is still possible to add the contributions to the probability of different resonance regions if the latter are independent (i.e., the resonance regions are isolated from each other in time).